An entropy stable essentially oscillation-free discontinuous Galerkin method for solving ideal magnetohydrodynamic equations*

Yong Liu†, Jianfang Lu‡, and Chi-Wang Shu§

Abstract. Recently, we developed an innovative entropy-stable oscillation-free discontinuous Galerkin (OFDG) scheme, referred to as ESOFDG, for hyperbolic conservation laws [Y. Liu, J. Lu, & C.-W. Shu, SIAM J. Sci. Comput. 46(2024), pp. A1132–A1159]. Through the incorporation of a strategically designed damping term, this scheme can effectively suppress the numerical oscillations without compromising high-order accuracy. Building on this foundation, in this paper we extend the ESOFDG framework to the ideal compressible magnetohydrodynamic (MHD) equations. Unlike the conventional hyperbolic conservation laws, the MHD system is usually subject to an additional divergence-free constraint, and the wave structure is not immediately apparent from the MHD model of conservative form. To address this, we employ a modified MHD model that includes a non-conservative source term, originally introduced by Godunov [S. K. Godunov, Numer. Methods Mech. Contin. Media, 1(1972), pp. 26–34], to establish appropriate entropy pairs. Additionally, we have carefully designed a damping term specifically tailored for the MHD equations in the ESOFDG framework. The resulting scheme not only maintains high-order accuracy and ensures entropy stability at the semi-discrete level, but also satisfies the properties of affine invariance and evolution invariance. Several numerical experiments are shown to confirm the robustness and efficiency of the proposed scheme for MHD equations.

Key words. Ideal magnetohydrodynamic equations; Entropy stability; Oscillation-free; Discontinuous Galerkin

AMS classification. 35L65, 65M12, 65M60, 76W05

*The first author's research is partially supported by NSFC grant 12201621, 12288201, the Youth Innovation Promotion Association (CAS), and Strategic Priority Research Program of the Chinese Academy of Sciences under the Grant No. XDB0640000. The second author's research is partially supported by the Fundamental Research Funds for the Central Universities 2024ZYGXZR049 and Science and Technology Program of Guangzhou 2023A04J1300. The third author's research is partially supported by NSF grant DMS-2309249.

†LSEC, Institute of Computational Mathematics, Academy of Mathematics and System Sciences and School of Mathematical Science, University of Chinese Academy of Sciences, Chinese Academy of Sciences, Beijing 100190, People's Republic of China. E-mail: yongliu@lsec.cc.ac.cn

‡School of Mathematics, South China University of Technology, Canton, Guangdong 510641, People's Republic of China. E-mail: jflu@scut.edu.cn. Corresponding author.

§Division of Applied Mathematics, Brown University, Providence, RI 02912, USA. E-mail: chi-wang_shu@brown.edu

1 Introduction

The ideal magnetohydrodynamic (MHD) is a fluid model of perfectly conducting quasi-neutral plasmas. It simplifies the behavior of fluids by assuming high electrical conductivity and neglecting non-ideal effects such as viscosity and resistivity. The ideal MHD model has widespread applications in both scientific and engineering fields, including space physics, geophysics, astrophysics, and engineering. This prevalence has driven extensive research into developing numerical methods to approximate the hyperbolic conservation laws governing ideal MHD. For nonlinear hyperbolic conservation laws, it is well-known that shock waves or contact discontinuities may arise during evolution, regardless of the smoothness of the initial or boundary conditions. As a result, the solutions of nonlinear hyperbolic equations are understood in the distributional sense [22]. However, weak solutions often lack uniqueness and require additional admissible criteria, such as entropy conditions, in order to pick out the physically relevant solution among the weak solutions. In the meantime, we would like to develop numerical methods that inherently satisfy the second law of thermodynamics, termed as *entropy stability*, based on the work of [46, 16, 35, 34].

In recent decades, there has been extensive research on entropy stability in the literature. For first- and second-order numerical methods, Tadmor's entropy conservative and entropy stable fluxes provide a foundational framework [46, 47]. In the realm of high-order finite volume methods, the TeCNO scheme developed by Fjordholm, Mishra, and Tadmor stands out [22]. This scheme leverages high-order entropy conservative fluxes [29] and the sign property of essentially non-oscillatory (ENO) reconstruction [23] to achieve entropy stability. In recent years, significant progress has been made in entropy-stable discontinuous Galerkin (DG) methods. Notably, Chen and Shu [11] proposed an entropy-stable DG scheme on unstructured simplex meshes, employing specialized Gauss-Lobatto quadrature rules with collocated surface quadrature points and discrete operators which possess the multidimensional summation-by-parts (SBP) property [27, 18]. Several other entropy-stable DG methods within the SBP framework have also been developed [6, 7, 8, 9]. For a comprehensive overview of entropy-stable DG methods for systems of conservation laws, we refer the reader to [12]. Applications of these entropy-stable methods to the MHD equations can be found in [51, 10, 35, 3].

One of the key physical constraints to the ideal MHD equations is the second law of thermodynamics, which states that the thermodynamic entropy of a closed system can only increase or remain constant over time. Another physical constraint is the divergence-free condition on the magnetic field, which prohibits the existence of magnetic monopoles. Maintaining a divergence-free magnetic field in numerical simulations of ideal MHD is a significant challenge, leading to the development of various techniques, including the projection method [4], the constraint transport (CT) method [20, 1], non-

staggered CT methods [21, 26, 41], the use of the magnetic vector potential $\mathbf{B} = \nabla \times \mathbf{A}$ [28], and exactly divergence-free methods [31, 2]. In this work, we adopt the widely used divergence cleaning method introduced by Munz et al. [37] and Dedner et al. [15]. This method augments the MHD system with a generalized Lagrange multiplier (GLM), which is advected and damped to suppress divergence errors. The resulting augmented system is known as the GLM-MHD system. It is important to note that while the GLM technique effectively reduces divergence errors, it does not eliminate them completely. Consequently, the GLM-MHD system incorporates non-conservative terms originating from Maxwell's equations when the divergence of the magnetic field is not exactly zero. These non-conservative terms play a crucial role in symmetrizing the system of PDEs and are essential for ensuring that the second law of thermodynamics is satisfied in the presence of non-zero divergence errors [10, 17, 35].

For hyperbolic conservation laws, high-order linear numerical schemes often generate spurious oscillations near discontinuities, known as the Gibbs phenomenon. These spurious oscillations can degrade accuracy in smooth regions, reduce the robustness of the schemes, and even cause potential code failures. The entropy-stable quadrature-based discontinuous Galerkin (DG) methods are not exempt from this issue, particularly for high Mach number flows. A common approach to reduce spurious oscillations is to apply slope limiters to the DG solutions, such as total variation diminishing (TVD) limiters and total variation bounded (TVB) limiters [14], and weighted ENO limiters [38, 56]. However, as noted in [11, Remark 4.4], designing entropy-stable TVD/TVB limiters for hyperbolic systems remains a challenge. Recently, we developed an alternative approach to control spurious oscillations by introducing artificial damping into the DG formulations [33, 36]. This method has proven effective in suppressing spurious oscillations while preserving key properties of the standard DG methods, such as conservation, optimal a priori error estimates, and superconvergence. In [34], we combine the entropy-stable DG framework with damping techniques to achieve both entropy stability and the oscillation-free property. Additionally, the OFDG method has been extended to other types of equations, including the shallow water equations [32], degenerate parabolic equations [48], and chemically reacting flows [19, 57].

Building upon our previous work in [34], this paper presents an extended algorithm for solving the MHD equations. We introduce a novel affine-invariant damping term specifically tailored for the MHD system, inspired by the oscillation-eliminating discontinuous Galerkin (OEDG) method proposed in [40]. Through rigorous theoretical analysis, we demonstrate that the resulting scheme retains the desirable properties of standard entropy-stable quadrature-based DG methods while simultaneously achieving entropy stability, divergence cleaning, and an essentially oscillation-free solution. The effectiveness of our proposed method is illustrated through a series of numerical experiments, which highlight its robust performance across various test cases.

The organization of the paper is as follows. In Section 2, we present the governing model along with its symmetrizable version incorporating Godunov's source term. Section 3 shows the construction of the entropy stable essentially oscillation-free DG method for the modified MHD equations. Numerical experiments are provided in Section 4, followed by concluding remarks in Section 5.

2 Ideal MHD equations

We consider the ideal magnetohydrodynamics (MHD) equations, which consist of a set of nonlinear hyperbolic equations, including compressible Euler equations and Maxwell equations. This system describes the conservation of mass, momentum, energy, and magnetic field of a particular fluid.

$$\begin{cases} \dfrac{\partial \rho}{\partial t} + \nabla \cdot (\rho \mathbf{u}) = 0, \\ \dfrac{\partial \rho \mathbf{u}}{\partial t} + \nabla \cdot \Big(\rho \mathbf{u}\mathbf{u}^T + \Big(p + \dfrac{|\mathbf{B}|^2}{2} \Big) \mathbb{I} - \mathbf{B}\mathbf{B}^T \Big) = \mathbf{0}, \\ \dfrac{\partial \mathbf{B}}{\partial t} + \nabla \cdot \big(\mathbf{u}\mathbf{B}^T - \mathbf{B}\mathbf{u}^T \big) = \mathbf{0}, \\ \dfrac{\partial E}{\partial t} + \nabla \cdot \Big(\Big(E + p + \dfrac{|\mathbf{B}|^2}{2} \Big) \mathbf{u} - (\mathbf{B} \cdot \mathbf{u}) \mathbf{B} \Big) = 0, \end{cases} \tag{2.1}$$

with an additional divergence constraint

$$\nabla \cdot \mathbf{B} = 0. \tag{2.2}$$

Here ρ is the density, $\mathbf{u} = [u_1, u_2, u_3]^T$ is the velocity field, p is the pressure, E is the total energy per unit volume, $\mathbf{B} = [B_1, B_2, B_3]^T$ is the magnetic field and $\mathbb{I} \in \mathbb{R}^{3\times 3}$ is the identity matrix. For the equation of state, we have

$$E = \frac{1}{2}\rho |\mathbf{u}|^2 + \frac{1}{2}|\mathbf{B}|^2 + \frac{p}{\gamma - 1},$$

where γ is the ratio of the specific heats. This system neglects the relativistic, viscous, and resistive effects, and the permeability is set to be unity. The divergence constraint (2.2) is satisfied for all time if the initial magnetic field is divergence-free, that is

$$\frac{\partial}{\partial t} \nabla \cdot \mathbf{B} = 0.$$

It is convenient to design numerical schemes for (2.1) based on the conservative form. We rewrite (2.1) into an abstract form

$$\frac{\partial \mathbf{W}}{\partial t} + \sum_{m=1}^{d} \frac{\partial \mathbf{f}_m(\mathbf{W})}{\partial x_m} = 0, \tag{2.3}$$

where $d = 3$ and

$$\begin{aligned}
\mathbf{W} &= [\rho, \rho u_1, \rho u_2, \rho u_3, B_1, B_2, B_3, E]^T, \\
\mathbf{f}_1 &= \Big[\rho u_1, \rho u_1^2 + p + \frac{1}{2}|\mathbf{B}|^2 - B_1^2, \rho u_1 u_2 - B_1 B_2, \rho u_1 u_3 - B_1 B_3, 0, \\
&\quad u_1 B_2 - u_2 B_1, u_1 B_3 - u_3 B_1, u_1\Big(E + p + \frac{1}{2}|\mathbf{B}|\Big) - B_1(u_1 B_1 + u_2 B_2 + u_3 B_3)\Big]^T, \\
\mathbf{f}_2 &= \Big[\rho u_2, \rho u_2 u_1 - B_2 B_1, \rho u_2^2 + p + \frac{1}{2}|\mathbf{B}|^2 - B_2^2, \rho u_2 u_3 - B_2 B_3, u_2 B_1 - u_1 B_2, 0, \\
&\quad u_2 B_3 - u_3 B_2, u_2\Big(E + p + \frac{1}{2}|\mathbf{B}|\Big) - B_2(u_1 B_1 + u_2 B_2 + u_3 B_3)\Big]^T. \\
\mathbf{f}_3 &= \Big[\rho u_3, \rho u_3 u_1 - B_3 B_1, \rho u_3 u_2 - B_3 B_2, \rho u_3^2 + p + \frac{1}{2}|\mathbf{B}|^2 - B_3^2, u_3 B_1 - u_1 B_3, \\
&\quad u_3 B_2 - u_2 B_3, 0, u_3\Big(E + p + \frac{1}{2}|\mathbf{B}|\Big) - B_3(u_1 B_1 + u_2 B_2 + u_3 B_3)\Big]^T.
\end{aligned}$$

For nonlinear conservation laws, it is well known that shock waves or contact discontinuities can form within finite time, even if the initial or boundary conditions are smooth. Consequently, it is natural to seek weak solutions. However, weak solutions to conservation laws are generally not unique. For scalar problems, a unique weak solution can be obtained by imposing sufficient entropy conditions. In the case of systems, while uniqueness may not be guaranteed, it is still desirable for the weak solution to satisfy the entropy condition. Here, we introduce one definition of entropy conditions based on the concept of entropy pairs.

Definition 2.1. *A pair of functions* $\big(U(\mathbf{W}), \mathbf{F}(\mathbf{W})\big)$ *is called an entropy pair, if* U *is a convex function and* $\mathbf{F}(\mathbf{W}) = [F_1, \cdots, F_d]^T$ *satisfies*

$$F_m'(\mathbf{W}) = U'(\mathbf{W})\mathbf{f}_m'(\mathbf{W}), \quad m = 1, \cdots, d, \tag{2.4}$$

where $U'(\mathbf{W})$ *and* $F_m'(\mathbf{W})$ *are viewed as row vectors,* $\mathbf{f}_m'(\mathbf{W})$ *is the Jacobian matrix. The* F_m, $m = 1, \cdots, d$, *are called the entropy fluxes.*

With the definition of entropy pairs, we have the additional admissibility condition to define the entropy solution.

Definition 2.2. *For any entropy pair* $\big(U(\mathbf{W}), \mathbf{F}(\mathbf{W})\big)$, *a weak solution* $\mathbf{W}$ *is an entropy solution of* (2.3) *if the following inequality holds:*

$$\frac{\partial U}{\partial t} + \sum_{m=1}^{d} \frac{\partial F_m}{\partial x_m} \le 0 \tag{2.5}$$

in the sense of distribution.

There is a close connection between the existence of an entropy pair and the symmetrization of a system of conservation laws.

Definition 2.3. *The system of conservation laws* (2.3) *is said to be symmetrizable if there exists a change of variables* $\mathbf{W} \to \mathbf{V}$ *which symmetrizes it, i.e. the equation* (2.3) *becomes*

$$\frac{\partial \mathbf{W}}{\partial \mathbf{V}} \frac{\partial \mathbf{V}}{\partial t} + \sum_{m=1}^{d} \frac{\partial \mathbf{f}_m}{\partial \mathbf{W}} \frac{\partial \mathbf{W}}{\partial \mathbf{V}} \frac{\partial \mathbf{V}}{\partial x_m} = 0, \tag{2.6}$$

where $\frac{\partial \mathbf{W}}{\partial \mathbf{V}}$ *is a symmetric positive definite matrix and* $\frac{\partial \mathbf{f}_m}{\partial \mathbf{W}} \frac{\partial \mathbf{W}}{\partial \mathbf{V}}$ *are symmetric matrices.*

Theorem 2.1. *(Mock) A necessary and sufficient condition for the system* (2.3) *to possess a strictly convex entropy* $U(\mathbf{W})$ *is that there exists a change of dependent variables* $\mathbf{V} = \mathbf{V}(\mathbf{W})$ *that symmetrizes* (2.3)*. (The proof can be found in, e.g. [24].)*

However, the original form of the ideal MHD equation can hardly be symmetrized. Fortunately, with the divergence-free constraint, the ideal MHD equations can be modified to achieve the symmetrization of systems [25, 39].

$$\frac{\partial \mathbf{W}}{\partial t} + \sum_{m=1}^{d} \frac{\partial \mathbf{f}_m}{\partial x_m} + \mathbf{S}(\mathbf{W}) \nabla \cdot \mathbf{B} = 0, \tag{2.7}$$

where $\mathbf{S}(\mathbf{W}) = [0, \mathbf{B}, \mathbf{u}, \mathbf{u} \cdot \mathbf{B}]^T$, and the added term $\mathbf{S}(\mathbf{W}) \nabla \cdot \mathbf{B}$ is termed as *Godunov's source term*. Due to the fact $\nabla \cdot \mathbf{B} = 0$, the above modification is consistent. Now we introduce the thermodynamic entropy [10]

$$U = -\frac{\rho s}{\gamma - 1}, \quad F_m = -\frac{\rho s u_m}{\gamma - 1}, \quad s = \ln(p \rho^{-\gamma}). \tag{2.8}$$

The entropy variables corresponding to the above entropy function are given by

$$\mathbf{V} = U'(\mathbf{W})^T = \left[\frac{\gamma - s}{\gamma - 1} - \beta |\mathbf{u}|^2, 2\beta \mathbf{u}, 2\beta \mathbf{B}, -2\beta\right]^T, \quad \beta = \frac{\rho}{2p}.$$

The change of variable $\mathbf{W} \to \mathbf{V}$ symmetrizes the equations (2.7). In terms of the components of $\mathbf{V}$, Godunov's source term can be written as the gradient of a function

$$\phi'(\mathbf{V}) = \mathbf{S}(\mathbf{W}),$$

where ϕ is given as

$$\phi(\mathbf{V}) = -\frac{V_2 V_5 + V_3 V_6 + V_4 V_7}{V_8} = 2\beta(\mathbf{u} \cdot \mathbf{B}) \tag{2.9}$$

which is homogeneous of degree one, i.e. $\mathbf{V} \cdot \phi'(\mathbf{V})^T = \phi(\mathbf{V})$.
The corresponding potential function and potential fluxes are given by

$$\begin{aligned} \varphi(\mathbf{V}) &= \mathbf{W} \cdot \mathbf{V} - U = \rho + \beta |\mathbf{B}|^2, \\ \psi_m(\mathbf{V}) &= \mathbf{V} \cdot \mathbf{f}_m(\mathbf{W}(\mathbf{V})) + \phi(\mathbf{V}) B_m - F_m = \rho u_m + \beta u_m |\mathbf{B}|^2, \end{aligned}$$

which satisfy

$$\varphi(\mathbf{V}) = \mathbf{W} \cdot \mathbf{V} - U, \quad \psi_m(\mathbf{V}) = \mathbf{V} \cdot \psi_m'(\mathbf{V}) - F_m.$$

3 Entropy stable OFDG methods

In this section, we proceed to present the entropy-stable oscillation-free discontinuous Galerkin (ESOFDG) scheme for the modified MHD equations. For simplicity, we focus on the one-dimensional case, and this framework can be directly extended to multi-dimensional structural meshes, like two-dimensional rectangular meshes and three-dimensional hexahedron meshes through tensor product techniques. For general unstructured meshes, we refer to entropy-stable DG schemes for the simplex meshes in [34]. First, we will review the entropy stable DG scheme for the modified MHD equations as presented in [35] which serves as a foundational building block.

3.1 Entropy stable DG methods

Now we consider the spatial discretization of the following equations

$$\frac{\partial \mathbf{W}}{\partial t}+\frac{\partial \mathbf{f}_1}{\partial x}+\mathbf{S}(\mathbf{W})\frac{\partial B_1}{\partial x}=0,\quad (x,t)\in(a,b)\times(0,T], \tag{3.1}$$

with the assumption of periodic or compactly supported boundary conditions. To introduce the entropy stable DG scheme for (3.1), we start with the mesh

$$a=x_{\frac{1}{2}}<x_{\frac{3}{2}}<\cdots<x_{N+\frac{1}{2}}=b,\quad I_j=\big(x_{j-\frac{1}{2}},x_{j+\frac{1}{2}}\big),\quad h_j=x_{j+\frac{1}{2}}-x_{j-\frac{1}{2}}$$

and the finite element space of polynomial degree k

$$\mathbf{V}_h^k=\big\{\mathbf{W}_h:\mathbf{W}_h|_{I_j}\in[\mathcal{P}^k(I_j)]^8,\quad 1\le j\le N\big\}$$

where $\mathcal{P}^k(I_j)$ is the space of polynomials of degree at most k over the subintervals I_j. We also introduce the commonly used notations in the standard DG method: for any $\mathbf{Q}_h\in\mathbf{V}_h^k$,

$$\{\mathbf{Q}_h\}_{j+\frac{1}{2}}=\frac{1}{2}\Big(\mathbf{Q}_h\big(x_{j+\frac{1}{2}}^-\big)+\mathbf{Q}_h\big(x_{j+\frac{1}{2}}^+\big)\Big),\quad [\![\mathbf{Q}_h]\!]_{j+\frac{1}{2}}=\mathbf{Q}_h\big(x_{j+\frac{1}{2}}^+\big)-\mathbf{Q}_h\big(x_{j+\frac{1}{2}}^-\big),$$

where $\mathbf{Q}_h\big(x_{j+\frac{1}{2}}^\pm\big)=\lim\limits_{\varepsilon\to0^+}\mathbf{Q}_h\big(x_{j+\frac{1}{2}}\pm\varepsilon\big)$. Then the standard DG method is to find $\mathbf{W}_h\in\mathbf{V}_h^k$ such that, for any $\mathbf{Q}_h\in\mathbf{V}_h^k$ and $1\le j\le N$

$$\begin{aligned}\int_{I_j}\frac{\partial \mathbf{W}_h}{\partial t}\cdot\mathbf{Q}_h\,\mathrm{d}x=&\int_{I_j}\mathbf{f}_1(\mathbf{W}_h)\cdot\frac{\partial \mathbf{Q}_h}{\partial x}\,\mathrm{d}x-\widehat{\mathbf{f}}_{1j+\frac{1}{2}}\cdot\mathbf{Q}_h\big(x_{j+\frac{1}{2}}^-\big)+\widehat{\mathbf{f}}_{1j-\frac{1}{2}}\cdot\mathbf{Q}_h\big(x_{j-\frac{1}{2}}^+\big)\\&-\int_{I_j}\mathbf{S}(\mathbf{W}_h)\cdot\mathbf{Q}_h\frac{\partial B_1}{\partial x}\,\mathrm{d}x-\frac{1}{2}\mathbf{S}\big(\mathbf{W}_h\big(x_{j+\frac{1}{2}}^-\big)\big)\cdot\mathbf{Q}_h\big(x_{j+\frac{1}{2}}^-\big)[\![B_1]\!]_{j+\frac{1}{2}}\\&-\frac{1}{2}\mathbf{S}\big(\mathbf{W}_h\big(x_{j-\frac{1}{2}}^+\big)\big)\cdot\mathbf{Q}_h\big(x_{j-\frac{1}{2}}^+\big)[\![B_1]\!]_{j-\frac{1}{2}}\end{aligned} \tag{3.2}$$

where $\widehat{\mathbf{f}}_{1j+\frac{1}{2}}$ is the numerical flux at $x_{j+\frac{1}{2}}$, depending on the values of numerical solution from both sides

$$\widehat{\mathbf{f}}_{1j+\frac{1}{2}} = \widehat{\mathbf{f}}_1\Big(\mathbf{W}_h\big(x^-_{j+\frac{1}{2}}\big), \mathbf{W}_h\big(x^+_{j+\frac{1}{2}}\big)\Big) \tag{3.3}$$

The non-conservative terms in (3.1) are discretized by using the treatment of the DG method for directly solving the Hamilton-Jacobi equations [13]. To achieve entropy stability, it needs to apply the Legendre-Gauss-Lobatto quadrature rule with $k_q + 1$ quadrature points to approximate three integrals in (3.2), $k_q \geq k$. Consider the reference interval $[-1, 1]$ associated with Gauss-Lobatto quadrature points $-1 = \xi_0 < \xi_1 < \cdots < \xi_{k_q} = 1$ and quadrature weights $\{w_i\}_{i=0}^{k_q}$. Let $\{L_\ell(x)\}_{\ell=0}^{k}$ be a set of basis functions of $\mathcal{P}^k(I)$. We define the polynomial differential matrix $\widehat{D} \in \mathbb{R}^{(k+1)\times(k+1)}$ such that

$$L'_\ell(x) = \sum_{r=0}^{k} \widehat{D}_{r\ell} L_r(x),$$

where $\widehat{D}_{r\ell}$ is the entry of the matrix $\widehat{D}$ at the r-th row and the ℓ-th column. The $\langle\cdot,\cdot\rangle$ and $\langle\cdot,\cdot\rangle_w$ stand for the continuous and discrete inner products, that is

$$\langle u, v\rangle = \int_{-1}^{1} uv \,\mathrm{d}\xi, \quad \langle u, v\rangle_w = \sum_{i=0}^{k_q} w_i u(\xi_i) v(\xi_i).$$

The mass matrix M is a diagonal matrix, i.e. $M = diag\{w_0, \cdots, w_{k_q}\} \in \mathbb{R}^{(k_q+1)\times(k_q+1)}$. According to integration by parts and algebraic accuracy of $\langle u, v\rangle_w$, we can obtain the summation-by-parts (SBP) property of modal matrices, that is

$$\widehat{M}\widehat{D} + \widehat{D}^T\widehat{M} = \widehat{B}, \tag{3.4}$$

where $\widehat{M}$ and $\widehat{B}$ are given as

$$\widehat{M} = V_k^T M V_k, \quad \widehat{B} = (V_k)^T B V_k, \tag{3.5}$$

where $V_k \in \mathbb{R}^{(k_q+1)\times(k+1)}$ is the Vandermonde matrix, whose columns are nodal values of $\{L_\ell(x)\}_{\ell=0}^{k}$ at quadrature points,

$$V_k = \begin{bmatrix} L_0(\xi_0) & \cdots & L_k(\xi_0) \\ \vdots & \ddots & \vdots \\ L_0(\xi_{k_q}) & \cdots & L_k(\xi_{k_q}) \end{bmatrix},$$

and the boundary matrix $B = diag\{-1, 0, \cdots, 0, 1\} = diag\{\tau_0, \cdots, \tau_{k_q}\} \in \mathbb{R}^{(k_q+1)\times(k_q+1)}$. To obtain the difference matrix, we need to define the L^2 projection matrix P_k:

$$P_k = \widehat{M}^{-1} V_k^T M. \tag{3.6}$$

Then the difference matrix $D \in \mathbb{R}^{(k_q+1)\times(k_q+1)}$ is defined as follows

$$D = \frac{1}{2}M^{-1}(\mathbb{I} + V_k P_k)^T B(\mathbb{I} - V_k P_k) + V_k \widehat{D} P_k, \tag{3.7}$$

where $\mathbb{I} \in \mathbb{R}^{(k_q+1)\times(k_q+1)}$ is the identity matrix. Since we use the Legendre-Gauss-Lobatto quadrature rule, which has collocated boundary points, we just use a simple restriction for the extrapolation matrix in (3.7). For general quadrature rules, one can refer to [12] for other choices of the extrapolation matrix. From [12, Theorem 3.1], we have the following SBP property

$$S + S^T = B, \quad S = MD, \tag{3.8}$$

which is a discrete analog of integration by parts. We define the affine mapping $x_j(\xi)$ from the reference interval to I_j: $x_j(\xi) = \frac{1}{2}(x_{j+\frac{1}{2}} + x_{j-\frac{1}{2}}) + \frac{\xi}{2}h_j$. The nodal values of numerical solutions are denoted by

$$\mathbf{W}_h^i = \mathbf{W}_h(x_j(\xi_i)),\ B_1^i = B_1(x_j(\xi_i)),\ \mathbf{f}_1^i = \mathbf{f}_1(x_j(\xi_i)),\ \mathbf{S}^i = \mathbf{S}(\mathbf{W}_h(x_j(\xi_i))),\ i = 0, \dots, k_q.$$

We also denote

$$\mathbf{f}_{1\star}^0 = \widehat{\mathbf{f}}_{1j-\frac{1}{2}}, \quad \mathbf{f}_{1\star}^k = \widehat{\mathbf{f}}_{1j+\frac{1}{2}}, \quad \mathbf{f}_{1\star}^i = \mathbf{0},\ i = 1, \dots, k_q - 1. \tag{3.9}$$

$$\begin{aligned} &\mathbf{g}^0 = \frac{1}{2}\mathbf{S}\big(\mathbf{W}_h\big(x_{j-\frac{1}{2}}^+\big)\big)[\![B_1]\!]_{j-\frac{1}{2}}, \quad \mathbf{g}^{k_q} = \frac{1}{2}\mathbf{S}\big(\mathbf{W}_h\big(x_{j+\frac{1}{2}}^-\big)\big)[\![B_1]\!]_{j+\frac{1}{2}}, \\ &\mathbf{g}^i = \mathbf{0},\ i = 1, \dots, k_q - 1. \end{aligned} \tag{3.10}$$

Then the semi-discrete entropy stable nodal DG scheme for (3.1) is given by

$$\begin{aligned} \frac{h}{2}\frac{\mathrm{d}}{\mathrm{d}t}\mathbf{W}_h^i + 2\sum_{\ell=0}^{k_q} D_{i\ell}\mathbf{f}_{1S}(\mathbf{W}_h^i, \mathbf{W}_h^\ell) + \sum_{\ell=0}^{k_q} D_{i\ell}\mathbf{S}^i B_1^\ell \\ = \frac{\tau_i}{w_i}(\mathbf{f}_1^i - \mathbf{f}_{1\star}^i) + \frac{\tau_i}{w_i}\mathbf{g}^i, \quad i = 0, \dots, k_q. \end{aligned} \tag{3.11}$$

Here, the DG scheme (3.11) is defined on the element I_j and the script j is omitted without causing any ambiguities. $\mathbf{f}_{1S}(\mathbf{W}_h^i, \mathbf{W}_h^\ell)$ and $\widehat{\mathbf{f}}_1$ are respectively the entropy conservative flux and entropy stable flux proposed by Chandrashekar and Klingenberg [10].

Definition 3.1. *A consistent, symmetric two-point numerical flux $\mathbf{f}_S(\mathbf{W}^L, \mathbf{W}^R)$ is entropy conservative for a given entropy function U if*

$$(\mathbf{V}^R - \mathbf{V}^L) \cdot \mathbf{f}_S(\mathbf{W}^L, \mathbf{W}^R) + (\phi^R - \phi^L)\frac{B_1^R + B_1^L}{2} = \psi^R - \psi^L \tag{3.12}$$

where $\mathbf{V}^{R,L}, \phi^{R,L}, B_1^{R,L}$, and $\psi^{R,L}$ are the entropy variables, the function defined in (2.9)*, magnetic field B_1 and potential fluxes $\psi(\mathbf{V})$ at the left and right states.*

Definition 3.2. *A consistent two-point numerical flux* $\widehat{\mathbf{f}}(\mathbf{W}^L, \mathbf{W}^R)$ *is entropy stable for a given entropy function* U *if*

$$(\mathbf{V}^R - \mathbf{V}^L) \cdot \mathbf{f}_S(\mathbf{W}^L, \mathbf{W}^R) + (\phi^R - \phi^L)\frac{B_1^R + B_1^L}{2} - (\psi^R - \psi^L) \leq 0. \tag{3.13}$$

A particular choice of the entropy conservative flux for MHD equations is proposed in [10], which is defined as follows:

$$\begin{aligned}
f_{1S}^{(1)} =& \hat{\rho}\{u_1\},\\
f_{1S}^{(2)} =& \frac{\{\rho\}}{2\{\beta\}} + \{u_1\}f_{1S}^{(1)} + \frac{1}{2}\{|\mathbf{B}|^2\} - \{B_1\}\{B_1\},\\
f_{1S}^{(3)} =& \{u_2\}f_{1S}^{(1)} - \{B_1\}\{B_2\},\\
f_{1S}^{(4)} =& \{u_3\}f_{1S}^{(1)} - \{B_1\}\{B_3\},\\
f_{1S}^{(5)} =& 0,\\
f_{1S}^{(6)} =& \frac{1}{\{\beta\}}(\{\beta u_1\}\{B_2\} - \{\beta u_2\}\{B_1\}),\\
f_{1S}^{(7)} =& \frac{1}{\{\beta\}}(\{\beta u_1\}\{B_3\} - \{\beta u_3\}\{B_1\}),\\
f_{1S}^{(8)} =& \frac{1}{2}\left(\frac{1}{(\gamma-1)\hat{\beta}} - \{|\mathbf{u}|^2\}\right) f_{1S}^{(1)} + \{u_1\}f_{1S}^{(2)} + \{u_2\}f_{1S}^{(3)} + \{u_3\}f_{1S}^{(4)},\\
&+ \{B_1\}f_{1S}^{(5)} + \{B_2\}f_{1S}^{(6)} + \{B_3\}f_{1S}^{(7)} - \frac{1}{2}\{u_1\}\{|\mathbf{B}|^2\}\\
&+ (\{u_1\}\{B_1\} + \{u_2\}\{B_2\} + \{u_3\}\{B_3\})\{B_1\},
\end{aligned}$$

where $\hat{(\cdot)}$ is logarithmic average of two strictly positive quantities as

$$\hat{\alpha} = \frac{\alpha_r - \alpha_l}{\ln \alpha_r - \ln \alpha_l}.$$

The entropy conservative flux for systems is not unique, we also refer to [51] for another entropy conservative flux for MHD equations. For the entropy stable flux, one can add dissipation to the entropy conservative fluxes in terms of the entropy variables to ensure the entropy inequality (3.13), that is

$$\widehat{\mathbf{f}}(\mathbf{W}^L, \mathbf{W}^R) = \mathbf{f}_S(\mathbf{W}^L, \mathbf{W}^R) - \frac{1}{2}\mathbf{D}[\![\mathbf{V}]\!]$$

where $\mathbf{D}$ is a suitable dissipation operator, e.g. [16, 50, 17]. Note that a careful evaluation of the dissipation matrix at the interface is needed for strong shocks or high Mach number flows. We choose the dissipation term $\mathbf{D}$ to be

$$\mathbf{D}_{LF} = |\lambda_{\max}^{\text{global}}|\boldsymbol{\mathcal{H}},$$

where $\lambda_{\max}^{\text{global}}$ is the largest eigenvalue of the ideal MHD system in the whole computational domain and $\boldsymbol{\mathcal{H}}$ is a discrete entropy Jacobian $\frac{\partial \mathbf{W}}{\partial \mathbf{V}}$. The entries of matrix $\boldsymbol{\mathcal{H}}$ are derived in [16, Section 4] for the ideal MHD equations such that the relation $[\![\mathbf{W}]\!] = \boldsymbol{\mathcal{H}}[\![\mathbf{V}]\!]$ holds. Therefore, this treatment leads to the Lax-Friedrichs (LF) flux at the interface of elements. The LF flux is advantageous because it is quite stable numerically and easy to implement, but it introduces excessive numerical dissipation due to its global nature. To reduce the diffusion of LF flux appropriately, we recommend to use the local Lax-Friedrichs (LLF) stabilization term instead of a global term

$$\mathbf{D}_{LF} = |\lambda_{\max}^{\text{local}}|\boldsymbol{\mathcal{H}}, \text{ with } \lambda_{\max}^{\text{local}} = \max\{\lambda_{\max}^{L}, \lambda_{\max}^{R}\}. \tag{3.14}$$

The following theorem established the semi-discrete scheme (3.11) is entropy stable if the interface numerical fluxes are entropy stable. We refer to [35] for the proof and omit it here.

Theorem 3.1. *If the numerical flux* $\widehat{\mathbf{f}}_1$ *at the element interface is entropy stable, then the scheme* (3.11) *is entropy stable.*

3.2 Entropy stable OFDG methods

As mentioned in [35], when the strong shocks appear, special stabilizing treatments are needed to reduce the numerical oscillations, such as the TVD/TVB limiter [43, 44]. However, in general, the TVD/TVB limiter for systems is not guaranteed to be entropy stable, see [11, Remark 3.4]. Recently, by using the damping technique, we proposed a framework of entropy stable essentially OFDG scheme [34] that is dissipative for any given entropy function without compromising high-order accuracy. We apply this framework to solve MHD equations (3.1) with some modifications of damping coefficients as follows:

$$\begin{aligned}\frac{h}{2}\frac{\mathrm{d}}{\mathrm{d}t}\mathbf{W}_h^i + 2\sum_{\ell=0}^{k_q} D_{i\ell}\mathbf{f}_{1S}(\mathbf{W}_h^i, \mathbf{W}_h^\ell) + \Big(\sum_{\ell=0}^{k_q} D_{i\ell}B_1^\ell\Big)\mathbf{S}^i \\ = \frac{\tau_i}{w_i}(\mathbf{f}_1^i - \mathbf{f}_{1\star}^i) + \frac{\tau_i}{w_i}\mathbf{g}^i - \sigma(\mathbf{W}_h)\Big(\mathbf{W}_h^i - \frac{1}{2}\sum_{\ell=0}^{k_q}\mathbf{W}_h^\ell w_\ell\Big),\end{aligned} \tag{3.15}$$

where the damping coefficient $\sigma(\mathbf{W}_h)$ is defined as follows:

$$\sigma(\mathbf{W}_h) = \begin{cases} \lambda_{\max}^{\text{local}}\dfrac{1}{\mathcal{M}_j^2}\max\limits_{1\le s\le 8}\displaystyle\sum_{\ell=0}^{1}\frac{1}{2}\big([\![\partial_x^\ell(\mathbf{W}_h)_s]\!]_{j-\frac{1}{2}}^2 + [\![\partial_x^\ell(\mathbf{W}_h)_s]\!]_{j+\frac{1}{2}}^2\big), & \mathcal{M}_j > \varepsilon, \\ 0, & \mathcal{M}_j \le \varepsilon, \end{cases} \tag{3.16}$$

where $\lambda_{\max}^{\text{local}} = \max\limits_{1\le s\le 8}|\lambda_s|$, with λ_s stands for s-th characteristic speed of the ideal MHD system in subcell I_j. $\mathcal{M}_j \triangleq \max\limits_{1\le s\le 8}\big\|(\mathbf{W}_h)_s - \big(\overline{(\mathbf{W}_h)_s}\big)_{\Omega_j}\big\|_{L^\infty(\Omega_j)}$, $\Omega_j = I_{j-1}\cup I_j\cup I_{j+1}$.

$(\mathbf{W}_h)_s$ is the s-th component of $\mathbf{W}_h$, $s = 1, \ldots, 8$, and $\big(\overline{(\mathbf{W}_h)_s}\big)_{\Omega_j}$ is the average of $(\mathbf{W}_h)_s$ on Ω_j. ε is a parameter to avoid division by zero. Compared to the damping coefficient $\sigma(\mathbf{W}_h)$ in [34], the proposed one here introduces the local characteristic speed, is free of the characteristic decomposition, and is evolution-invariant. Also, it becomes affine-invariant due to the denominator $\mathcal{M}_j$ being added. This kind of treatment is inspired by OEDG [40], and it is more robust, efficient, and easy to implement.

The next theorem states that (3.15) is entropy stable if the $\mathbf{f}_{1S}$ is entropy conservative and the numerical flux $\widehat{\mathbf{f}_1}$ is entropy stable at the element interface.

Theorem 3.2. *If $\mathbf{f}_{1S}$ is entropy conservative and $\widehat{\mathbf{f}_1}$ is entropy stable, then* (3.15) *is entropy stable. Moreover, the scheme is at least k-th order accurate measured by local truncation errors.*

Proof. Recall the proof of Theorem 3.2 in [35], we have

$$\frac{\mathrm{d}}{\mathrm{d}t}\sum_{i=0}^{k_q}\frac{h}{2}w_i U(\mathbf{W}_h^i) = \mathcal{F}^{k_q} - \mathcal{F}^0 - \sigma(\mathbf{W}_h)w_i\mathbf{V}_h^i\cdot\Big(\mathbf{W}_h^i - \frac{1}{2}\sum_{\ell=0}^{k_q}\mathbf{W}_h^\ell w_\ell\Big), \tag{3.17}$$

where $\mathcal{F}^0$ and $\mathcal{F}^{k_q}$ are

$$\mathcal{F}^0 = \big(\psi^0 - \mathbf{V}_h^0\cdot\mathbf{f}_{1\star}^0\big) - \phi^0\{B_1\}^0, \quad \mathcal{F}^{k_q} = \big(\psi^{k_q} - \mathbf{V}_h^{k_q}\cdot\mathbf{f}_{1\star}^{k_q}\big) - \phi^{k_q}\{B_1\}^{k_q}$$

and $\mathbf{V}_h^i$ is the value of the entropy variable at node $x_j(\xi_i)$, the ψ^i and ϕ^i are potential fluxes and homogeneous functions of the source term respectively. Since $U(\mathbf{W})$ is a convex function, we have

$$\big(U'(\mathbf{W}_1) - U'(\mathbf{W}_2)\big)\cdot(\mathbf{W}_1 - \mathbf{W}_2) \geq 0, \quad \forall\, \mathbf{W}_1, \mathbf{W}_2 \in \mathbb{R}^8. \tag{3.18}$$

By the orthogonality of the L^2 projection and (3.18), the last term in (3.17) becomes

$$\begin{aligned}
&-\sigma(\mathbf{W}_h)w_i\mathbf{V}_h^i\cdot\Big(\mathbf{W}_h^i - \frac{1}{2}\sum_{\ell=0}^{k_q}\mathbf{W}_h^\ell w_\ell\Big)\\
=&-\sigma(\mathbf{W}_h)w_i\Big(U'(\mathbf{W}_h^i) - U'\Big(\frac{1}{2}\sum_{\ell=0}^{k_q}\mathbf{W}_h^\ell w_\ell\Big)\Big)\cdot\Big(\mathbf{W}_h^i - \frac{1}{2}\sum_{\ell=0}^{k}\mathbf{W}_h^\ell w_\ell\Big) \leq 0.
\end{aligned}$$

Therefore, on the single element, we have

$$\frac{\mathrm{d}}{\mathrm{d}t}\sum_{i=0}^{k_q}\frac{h_j}{2}w_i U(\mathbf{W}_h^i) \leq \mathcal{F}^{k_q} - \mathcal{F}^0.$$

Sum it over $j = 1, \ldots, N$ and use the periodic boundary condition, we have

$$\frac{\mathrm{d}}{\mathrm{d}t}\sum_{j=1}^{N}\sum_{i=0}^{k_q}\frac{h}{2}w_i U(\mathbf{W}_h^i)$$

$$
\begin{aligned}
&\le \sum_{j=1}^{N} \big(\psi_j^{k_q} - (\mathbf{V}_h)_j^{k_q} \cdot \widehat{\mathbf{f}}_{1,j+\frac{1}{2}}\big) - \phi_j^{k_q}\{B_1\}_j^{k_q} - \big(\psi_{j+1}^0 - (\mathbf{V}_h)_{j+1}^0 \cdot \widehat{\mathbf{f}}_{1,j+\frac{1}{2}}\big) + \phi_{j+1}^0\{B_1\}_{j+1}^0 \\
&\le \sum_{j=1}^{N} \big((\mathbf{V}_h)_{j+1}^0 - (\mathbf{V}_h)_j^{k_q}\big) \cdot \widehat{\mathbf{f}}_{1,j+\frac{1}{2}}\big((\mathbf{W}_h)_j^{k_q}, (\mathbf{W}_h)_{j+1}^0\big) - \big(\psi_{j+1}^0 - \psi_j^{k_q}\big) \\
&\qquad + \{B_1\}_{j+\frac{1}{2}}\big(\phi_{j+1}^0 - \phi_j^{k_q}\big) \\
&\le 0.
\end{aligned}
$$

The last inequality holds because $\widehat{\mathbf{f}}_{1,j+\frac{1}{2}}$ is the entropy stable flux defined in (3.13).

Accuracy: let $\widetilde{\mathbf{f}_{1S}}(x,y) = \mathbf{f}_{1S}(\mathbf{W}(x), \mathbf{W}(y))$ and $\widetilde{\mathbf{f}_1}(x) = \mathbf{f}_1(\mathbf{W}(x))$. Since $\mathbf{f}_{1S}(\cdot,\cdot)$ is symmetric and consistent, then $\widetilde{\mathbf{f}_{1S}}(x,x) = \widetilde{\mathbf{f}_1}(x)$. Hence we have

$$
\frac{\partial \widetilde{\mathbf{f}_1}}{\partial x}(x) = \frac{\partial \widetilde{\mathbf{f}_{1S}}}{\partial x}(x,x) + \frac{\partial \widetilde{\mathbf{f}_{1S}}}{\partial y}(x,x) = 2\frac{\partial \widetilde{\mathbf{f}_{1S}}}{\partial y}(x,x).
$$

Since the difference matrix D is exact for polynomials of degree up to k by (3.7),

$$
\begin{aligned}
\frac{4}{h}\sum_{\ell=0}^{k_q} D_{i\ell}\widetilde{\mathbf{f}_{1S}}(x_j(\xi_i), x_j(\xi_\ell)) &= 2\frac{\partial \widetilde{\mathbf{f}_{1S}}}{\partial y}(x_j(\xi_i), x_j(\xi_i)) + \mathcal{O}(h^k) \\
&= \frac{\partial \widetilde{\mathbf{f}_1}}{\partial x}(x_j(\xi_i)) + \mathcal{O}(h^k) = \frac{\partial \mathbf{f}_1}{\partial x}(\mathbf{W}(x_j(\xi_i))) + \mathcal{O}(h^k),
\end{aligned}
$$

and

$$
\frac{2}{h}\Big(\sum_{\ell=0}^{k_q} D_{i\ell}B_1(x_j(\xi_\ell))\Big)\mathbf{S}(\mathbf{W}(x_j(\xi_i))) = \frac{\partial B_1}{\partial x}(x_j(\xi_i))\mathbf{S}(\mathbf{W}(x_j(\xi_i))) + \mathcal{O}(h^k).
$$

By the consistency of the numerical flux $\widehat{\mathbf{f}_1}$ and the smoothness of $\mathbf{W}$, we have

$$
\begin{aligned}
&\mathbf{f}_1(\mathbf{W}(x_{j+\frac{1}{2}})) = \widehat{\mathbf{f}_1}_{j+\frac{1}{2}}, \quad [\![\partial_x^\ell(\mathbf{W})_s]\!]_{j+\frac{1}{2}} = 0, \quad \ell = 0, 1,\ s = 1, \dots, 8. \\
&\mathbf{g}(x_j(\xi_i)) = \mathbf{0}, \quad i = 0, \dots, k_q, \text{ and } \sigma(\mathbf{W}) = 0.
\end{aligned}
$$

Therefore, the local truncation error is of high order:

$$
\begin{aligned}
&\frac{\mathrm{d}}{\mathrm{d}t}\mathbf{W}(x_j(\xi_i), t) + \frac{4}{h}\sum_{\ell=0}^{k_q} D_{i\ell}\mathbf{f}_{1S}(\mathbf{W}(x_j(\xi_i), t), \mathbf{W}(x_j(\xi_\ell), t)) \\
&- \frac{2\tau_i}{hw_i}(\mathbf{f}_1(x_j(\xi_i)) - \mathbf{f}_{1\star}(x_j(\xi_i))) + \frac{2}{h}\Big(\sum_{\ell=0}^{k_q} D_{i\ell}B_1(x_j(\xi_\ell), t)\Big)\mathbf{S}(\mathbf{W}(x_j(\xi_i), t)) \\
&- \frac{2\tau_i}{hw_i}\mathbf{g}(x_j(\xi_i)) + \frac{2}{h}\sigma(\mathbf{W})\Big(\mathbf{W}(x_j(\xi_i), t) - \frac{1}{2}\sum_{\ell=0}^{k_q}\mathbf{W}(x_j(\xi_\ell), t)w_\ell\Big) \\
=&\frac{\partial \mathbf{W}}{\partial t}(x_j(\xi_i), t) + \frac{\partial \mathbf{f}_1}{\partial x}(\mathbf{W}(x_j(\xi_i), t)) + \frac{\partial B_1}{\partial x}(x_j(\xi_i), t)\mathbf{S}(\mathbf{W}(x_j(\xi_i), t)) + \mathcal{O}(h^k) \\
=&\mathcal{O}(h^k).
\end{aligned}
\tag{3.19}
$$

□

Remark 3.1. *We assume that numerical solutions for density and pressure in entropy fluxes are positive. However, for the ideal magnetohydrodynamics (MHD) equations, the provably positive-preserving (PP) property is inherently linked to the discrete divergence-free condition [52]. Since our entropy-stable framework lacks local divergence-freeness, developing a provably positive-preserving and entropy-stable DG scheme remains an open challenge. As a pragmatic workaround, we can employ the scaling limiter [55] in the computation and adaptively reduce time steps to enforce positivity, albeit heuristically. A rigorous, intrinsically positive scheme is still needed and awaits further innovation.*

3.3 Time discretization method

In this subsection, we continue to discretize the time variable for the semi-discrete scheme (3.15). For hyperbolic problems or convection-dominated problems, a class of high-order nonlinearly stable Runge-Kutta methods are widely used in temporal discretization. A notable feature of this class of time discretization methods is that they can preserve strong stability in some semi-norm (total variation semi-norm, maximum norm, etc.) from forward Euler stepping. We adopt the third-order total variation diminishing Runge-Kutta (TVDRK3) method [44, 45] as our time stepping method. Assume we have the semi-discrete scheme (3.15), denoted by

$$\frac{\mathrm{d}}{\mathrm{d}t}\mathbf{W}_h + \mathbf{D}_h[\mathbf{W}_h] + \frac{2}{h}\sigma(\mathbf{W}_h)\big(\mathbf{W}_h - \overline{(\mathbf{W}_h)}\big) = 0, \tag{3.20}$$

where $\mathbf{D}_h[\mathbf{W}_h]$ is the discretization of the flux term and source term, $\overline{(\mathbf{W}_h)}$ is the average of $\mathbf{W}_h$ in the element I_j. If we apply the TVDRK3 method to (3.20) and treat the damping term explicitly, it may lead to restricted CFL conditions. Therefore, we treat the damping term implicitly by splitting the forward Euler step into two steps. The fully discrete scheme from time level t_n to t_{n+1} is given as follows:

$$\begin{cases} \widetilde{\mathbf{W}}_h^{n,1} = \mathbf{W}_h^n - \tau\mathbf{D}_h[\mathbf{W}_h^n], \\ \mathbf{W}_h^{n,1} = \widetilde{\mathbf{W}}_h^{n,1} - \dfrac{2\tau}{h}\sigma\big(\widetilde{\mathbf{W}}_h^{n,1}\big)\big(\mathbf{W}_h^{n,1} - \overline{(\mathbf{W}_h^{n,1})}\big), \\ \widetilde{\mathbf{W}}_h^{n,2} = \dfrac{3}{4}\mathbf{W}_h^n + \dfrac{1}{4}\mathbf{W}_h^{n,1} - \dfrac{1}{4}\tau\mathbf{D}_h[\mathbf{W}_h^{n,1}], \\ \mathbf{W}_h^{n,2} = \widetilde{\mathbf{W}}_h^{n,2} - \dfrac{1}{4}\cdot\dfrac{2\tau}{h}\sigma\big(\widetilde{\mathbf{W}}_h^{n,2}\big)\big(\mathbf{W}_h^{n,2} - \overline{(\mathbf{W}_h^{n,2})}\big), \\ \widetilde{\mathbf{W}}_h^{n+1} = \dfrac{1}{3}\mathbf{W}_h^n + \dfrac{2}{3}\mathbf{W}_h^{n,2} - \dfrac{2}{3}\tau\mathbf{D}_h[\mathbf{W}_h^{n,2}], \\ \mathbf{W}_h^{n+1} = \widetilde{\mathbf{W}}_h^{n+1} - \dfrac{1}{3}\cdot\dfrac{2\tau}{h}\sigma\big(\widetilde{\mathbf{W}}_h^{n+1}\big)\big(\mathbf{W}_h^{n+1} - \overline{(\mathbf{W}_h^{n+1})}\big). \end{cases} \tag{3.21}$$

since the damping coefficient $\sigma\big(\widetilde{\mathbf{W}}_h\big)$ can be obtained explicitly, this kind of splitting avoids the nonlinear iteration. For instance, we can obtain $\mathbf{W}_h^{n,1}$ by

$$\mathbf{W}_h^{n,1} = \frac{1}{1+\alpha}\widetilde{\mathbf{W}}_h^{n,1} + \frac{\alpha}{1+\alpha}\overline{\big(\widetilde{\mathbf{W}}_h^{n,1}\big)}, \quad \alpha = \frac{2\tau}{h}\sigma\big(\widetilde{\mathbf{W}}_h^{n,1}\big).$$

4 Numerical tests

In this section, we present some numerical results to validate our theoretical results. We adopt the third-order total variation diminishing Runge-Kutta (TVDRK3) method (3.21) as our time stepping method presented in Section 3.3. Throughout the paper, the CFL number is $CFL = \frac{0.6}{(2k+1)}$ unless otherwise specified. We also take the degree of the piecewise polynomial space $k = 2$, and the number of quadrature rule points $k_q = k + 2$. The parameter ε in (3.16) is taken as 10^{-12} for both one- and two-dimensional problems. The computation in this section is partially supported by High Performance Computing Platform of South China University of Technology.

4.1 One-dimensional problems

Example 1. *This example considers a smooth problem with only one nontrivial component ρ, and it is essentially a scalar problem. The initial condition is given as*

$$\rho = 1 + 0.2\sin x,\ \mathbf{u} = [1, 0, 0]^T,\ \mathbf{B} = [0.5, 1.0, 1.5]^T,\ p = 2.$$

The solution is periodic in the domain $(0, 2\pi)$. The ratio of the specific heats is $\gamma = 5/3$, and the final time is $T = 1.3$.

We list the error of numerical solutions in L^1, L^2, and L^∞ norms in Table 1. We clearly observe the $(k + 1)$-th order convergence rates, which verify the damping term will not sacrifice the high-order accuracy for smooth solutions.

Table 1: Errors and orders in Example 1, $k = 2$, $T = 1.3$.

N	L^1 error	order	L^2 error	order	L^∞ error	order
12	1.085E-04	–	9.044E-05	–	1.580E-04	–
24	1.363E-05	2.993	1.130E-05	3.000	1.897E-05	3.059
48	1.696E-06	3.007	1.413E-06	3.000	2.365E-06	3.004
96	2.120E-07	3.000	1.766E-07	3.000	2.945E-07	3.005
192	2.650E-08	3.000	2.208E-08	3.000	3.676E-08	3.002
384	3.313E-09	3.000	2.760E-09	3.000	4.593E-09	3.001

Example 2. *We consider three shock tube problems in this example.*

(a) *The initial condition of the first Riemann problem is given as*

$$[\rho, u_1, u_2, u_3, B_1, B_2, B_3, p]^T = \begin{cases} [1.000, 0, 0, 0, 0.75, +1, 0, 1.0]^T, & x \le 0 \\ [0.125, 0, 0, 0, 0.75, -1, 0, 0.1]^T, & x > 0 \end{cases}$$

The ratio of the specific heats is $\gamma = 2$. The computational domain is $\Omega = (-1, 1)$ and the final time is $T = 0.2$.

(b) *The initial condition of the second Riemann problem is given as*

$$[\rho, u_1, u_2, u_3, B_1, B_2, B_3, p]^T = \begin{cases} [1.0, 0, 0, 0, 0.7, 0, 0, 1.0]^T, & x \leq 0 \\ [0.3, 0, 0, 1.0, 0.7, 1.0, 0, 0.2]^T, & x > 0 \end{cases}$$

The ratio of the specific heats is $\gamma = 5/3$. *The computational domain is* $\Omega = (-1, 1)$ *and the final time is* $T = 0.32$.

(c) *The initial condition of the third Riemann problem is given as*

$$[\rho, u_1, u_2, u_3, B_1, B_2, B_3, p]^T = \begin{cases} [1.000, 0, 0, 0, 0, 0, +1, 0, 1000]^T, & x \leq 0 \\ [0.125, 0, 0, 0, 0, 0, -1, 0, 0.100], & x > 0 \end{cases}$$

The ratio of the specific heats is $\gamma = 2$. *The computational domain is* $\Omega = (-1, 1)$ *and the final time is* $T = 0.012$.

The first Riemann problem (a), introduced by Brio and Wu in [5], demonstrates the formation of compound waves in MHD. We employ a uniform mesh of 800 cells to solve this problem, and the numerical solution at $T = 0.2$ is depicted in Fig. 1. To provide a reference solution, we utilize a simulation with 5000 cells. The numerical solution exhibits the following wave structures: left-moving waves consisting of a fast rarefaction wave and an intermediate shock attached to a slow rarefaction wave; and right-moving waves comprising a contact discontinuity, a slow shock, and a fast rarefaction wave. The ESOFDG scheme demonstrates satisfactory performance without generating significant spurious oscillations. The second Riemann problem (b), introduced by Ryu and Jones in [42], features a switch-on slow rarefaction. Switch-on/off magnetosonic waves cause the tangential magnetic field to turn on/off. From left to right, the numerical solution includes the hydrodynamic rarefaction, the switch on slow shock, the contact discontinuity, the slow Shock, the Alfvên/Rotation wave, and the fast rarefaction. The third Riemann problem (c) is used to evaluate the code for high Mach number flow. The numerical solution has good resolution with 200 cells.

4.2 Two-dimensional problems

Example 3. *This example describes a circularly polarized Alfvén wave moving in the domain* $(0, 1/\cos\alpha) \times (0, 1/\sin\alpha)$ *with periodic boundary conditions.* α *denotes the angle between the moving direction and the x-axis. The ratio of the specific heats is* $\gamma = 5/3$ *and the initial condition is given as*

$$\rho = 1, \quad u_1 = -v_\perp \sin\alpha, \quad u_2 = v_\perp \cos\alpha, \quad u_3 = 0.1\cos(2\pi x_\parallel),$$
$$B_1 = B_\parallel \cos\alpha - B_\perp \sin\alpha, \quad B_2 = B_\parallel \sin\alpha + B_\perp \cos\alpha, \quad B_3 = u_3, \quad p = 0.1,$$

Figure 1: *First Riemann problem* in Example 2, $N = 800$, $k = 2$, $T = 0.2$.

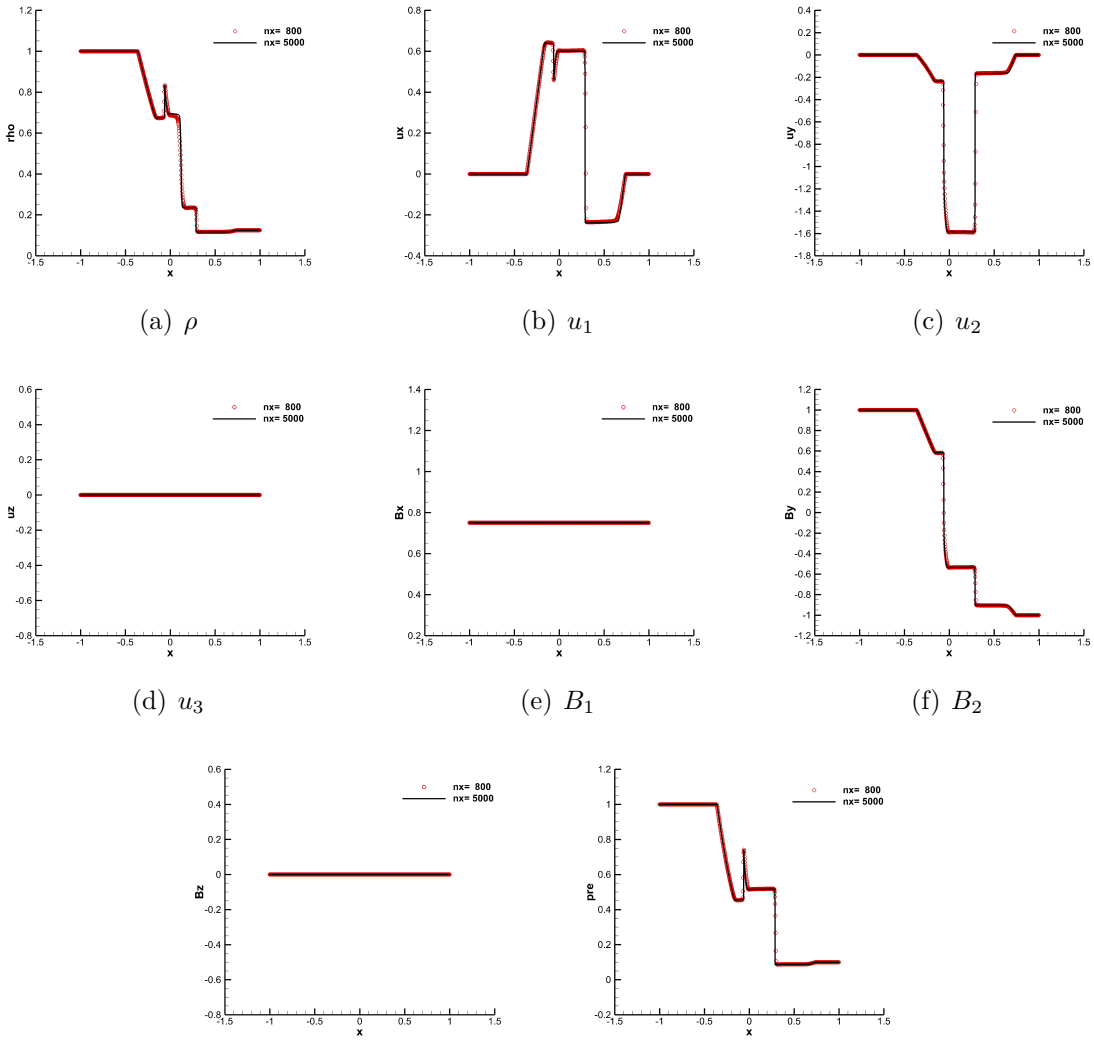

(a) ρ (b) u_1 (c) u_2

(d) u_3 (e) B_1 (f) B_2

(g) B_3 (h) p

with $B_{\parallel} = 1$, $B_{\perp} = v_{\perp} = 0.1\sin(2\pi x_{\parallel})$, $x_{\parallel} = x\cos\alpha + y\sin\alpha$. *The period of the example is* 1 *in time unit, and we compute the errors of* $B_{\perp}$ *in* L^1, L^2 *and* L^{∞} *norms at time* $T = 5$.

This example is taken in [49], and the solution has periodicity. We can see that the optimal order of error accuracy is obtained after 5 periodic times in Table 2.

Example 4. *This 2D Riemann problem was considered by Yee and Sjögreen in [54].Denote the four quadrants as:* I*:* $x > 0$, $y > 0$*;* II*:* $x < 0$, $y > 0$*;* III*:* $x < 0$, $y < 0$*;* IV*:* $x > 0$, $y < 0$. *The problem initially consists of four states in each quadrant, see Table 3. The domain is* $(-1, 1) \times (-1, 1)$ *with extrapolated boundary conditions. The adiabatic index is* $\gamma = 5/3$ *and the final time is* 0.2.

Figure 2: *Second Riemann problem* in Example 2, $N = 800$, $k = 2$, $T = 0.32$.

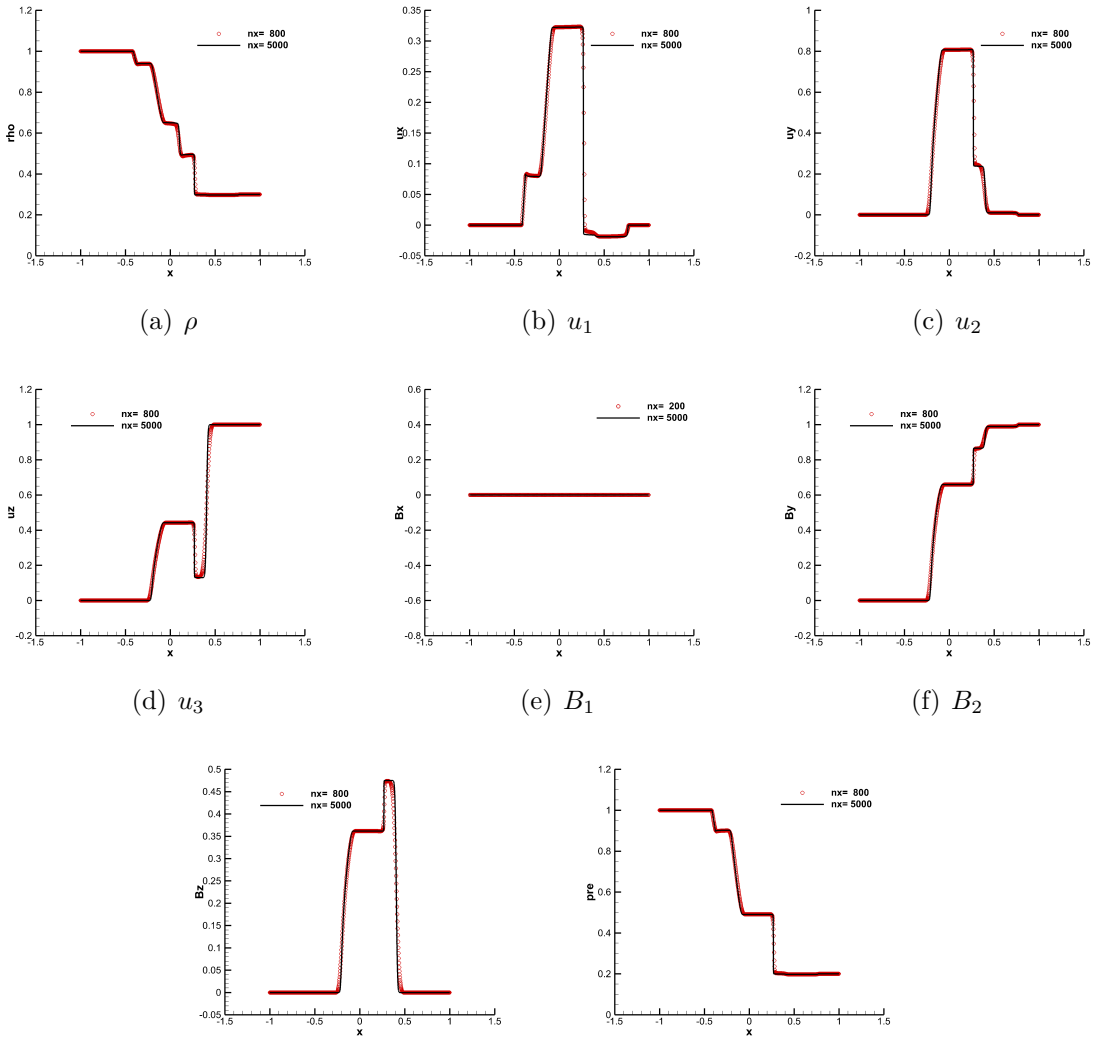

(a) ρ (b) u_1 (c) u_2

(d) u_3 (e) B_1 (f) B_2

(g) B_3 (h) p

Table 2: Errors and orders in Example 3, $k = 2$, $T = 5$.

$N_x \times N_y$	L^1 error	order	L^2 error	order	L^∞ error	order
16×16	9.706E-03	–	5.550E-03	–	5.575E-03	–
32×32	7.883E-04	3.622	4.709E-04	3.559	6.526E-04	3.095
64×64	2.356E-05	5.065	1.470E-05	5.002	3.207E-05	4.347
128×128	1.567E-06	3.910	9.752E-07	3.914	2.623E-06	3.612
256×256	1.846E-07	3.086	1.176E-07	3.051	3.245E-07	3.014
512×512	2.478E-08	2.897	1.628E-08	2.854	4.297E-08	2.917

We compute this example by using 128×128 and 256×256 meshes. The magnetic fields B_1 and B_2 are shown in Figure 4 with 30 equally spaced between 0.37 and 1.24 for

Figure 3: *Third Riemann problem* in Example 2, $N = 800$, $k = 2$, $T = 0.012$.

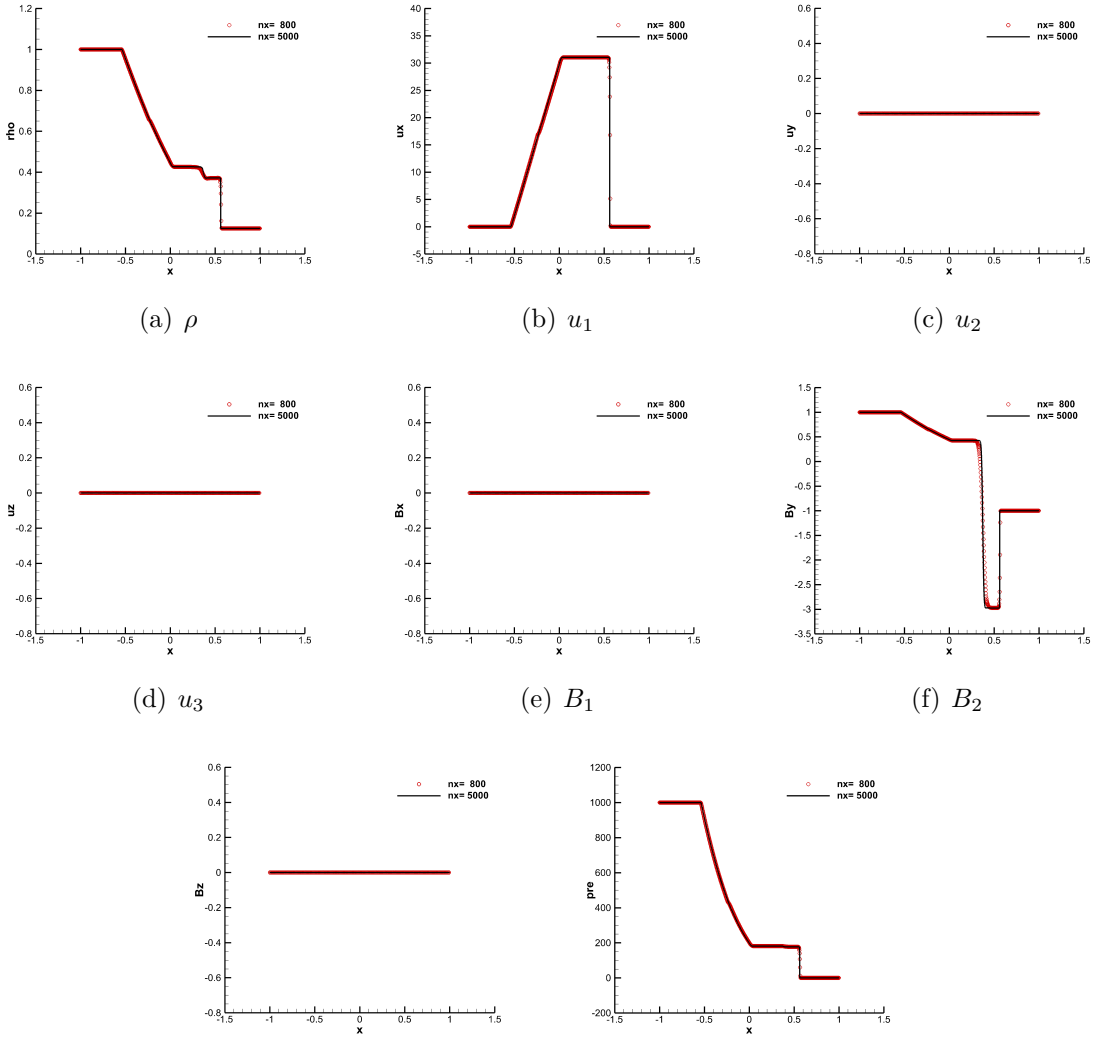

(a) ρ (b) u_1 (c) u_2

(d) u_3 (e) B_1 (f) B_2

(g) B_3 (h) p

Table 3: The initial data in Example 4

Quadrant	ρ	ρu_1	ρu_2	ρu_3	B_1	B_2	B_3	E
I	0.9308	1.4557	-0.4633	0.0575	0.3501	0.9830	0.3050	5.0838
II	1.0304	1.5774	-1.0455	-0.1016	0.3501	0.5078	0.1576	5.7813
III	1.0000	1.7500	-1.0000	0.0000	0.5642	0.5078	0.2539	6.0000
IV	1.8887	0.2334	-1.7422	0.0733	0.5642	0.9830	0.4915	12.999

B_1 and between 0.55 and 1.41 for B_2. The ESOFDG scheme obtains comparable results as shown in [54].

Figure 4: The profiles of magnetic fields B_1, B_2 of Riemann problem in Example 4, $k = 2$, $T = 0.2$. 30 equally spaced contour lines are plotted: magnetic field $B_1 \in [0.37, 1.24]$, magnetic field $B_2 \in [0.55, 1.41]$.

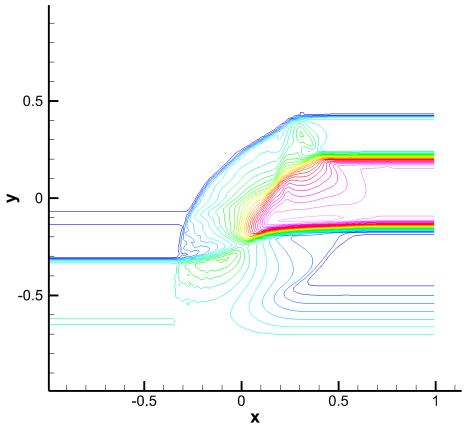

(a) B_1, 128×128

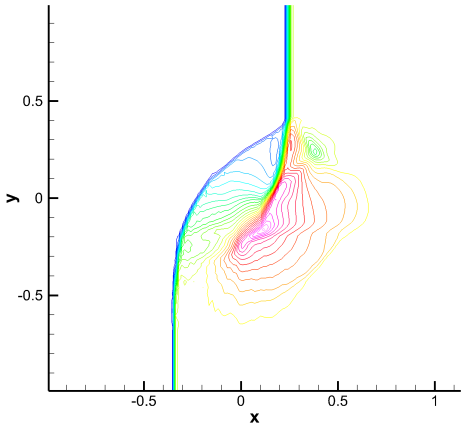

(b) B_2, 128×128

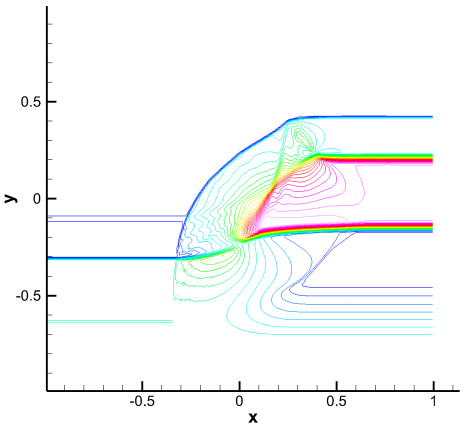

(c) B_1, 256×256

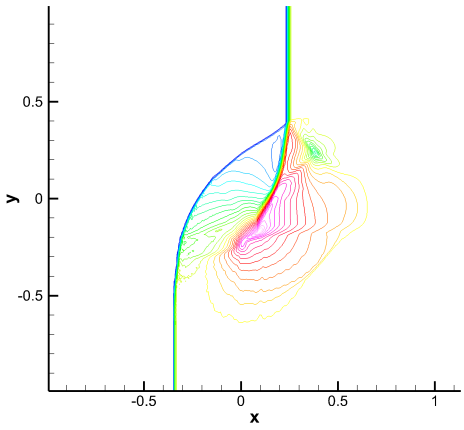

(d) B_2, 256×256

Example 5. *Consider the Orszag-Tang vortex evolution problem [10] with periodic boundary conditions. The initial condition is given as*

$$\rho = \frac{25}{36\pi},\ \mathbf{u} = [-\sin(2\pi x_2), \sin(2\pi x_1), 0]^T,\ \mathbf{B} = \frac{1}{\sqrt{4\pi}}[-\sin(2\pi x_2), \sin(4\pi x_1), 0]^T,\ p = \frac{5}{12\pi}.$$

The ratio of the specific heats is $\gamma = 5/3$. *The computational domain is* $\Omega = (0,1)\times(0,1)$ *and the final time is* $T = 0.5$.

This example is a widely used test problem in MHD simulations. We use uniform meshes to solve this problem. The density and pressure contour are shown in Figure 5 on meshes of size 128×128 and 256×256. The numerical scheme is stable on all the

meshes and Figure 6 shows that the discrete total entropy does not increase with time during the simulation. Although we cannot prove the entropy stability with explicit Runge-Kutta time discretization, the numerical evidence shows the total entropy which in principle should decrease with time if the scheme is entropy stable.

Figure 5: The profiles of density and thermal pressure of Orszag-Tang vortex problem in Example 5, $k = 2$, $T = 0.5$. 40 equally spaced contour lines are plotted: density $\rho \in [0.1, 0.48]$, thermal pressure $p \in [0.04, 0.49]$.

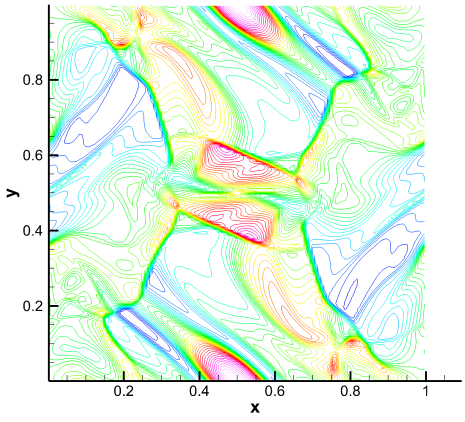

(a) ρ, 128×128

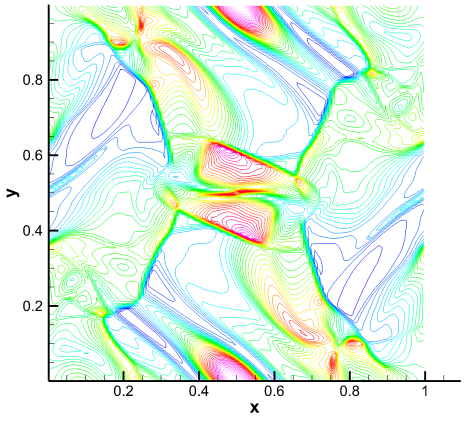

(b) p, 128×128

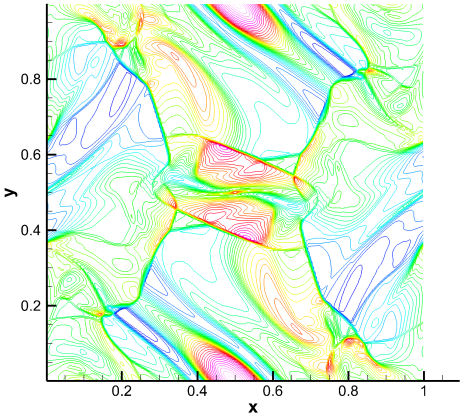

(c) ρ, 256×256

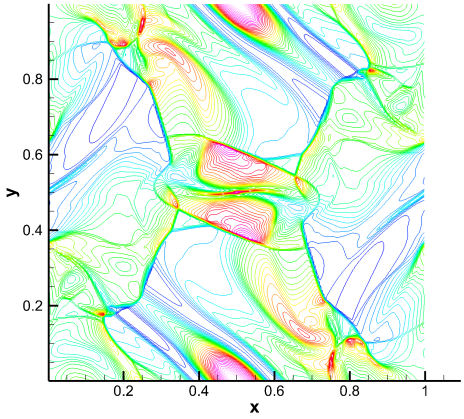

(d) p, 256×256

Example 6. *Consider the rotor problem with periodic boundary conditions. The initial*

Figure 6: The entropy of Orszag-Tang vortex problem in Example 5, $k = 2$, $T = 0.5$.

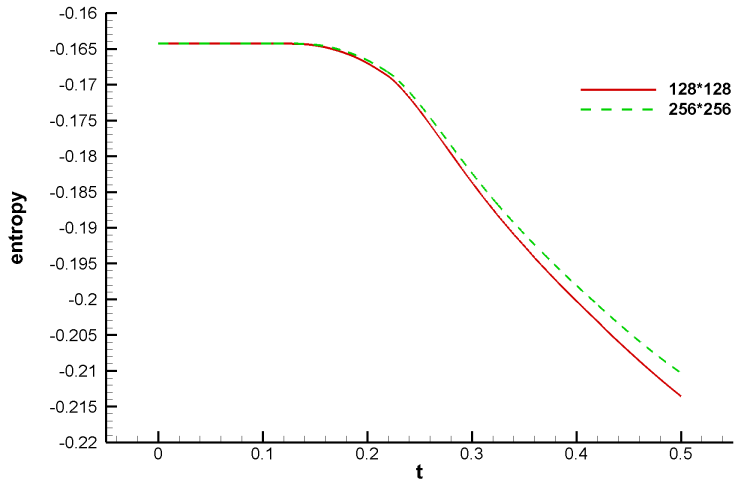

condition is given as

$$[\rho, u_1, u_2]^T = \begin{cases} \Big[10, -\dfrac{u_0}{r_0}(x_2 - 0.5), \dfrac{u_0}{r_0}(x_1 - 0.5)\Big]^T, & r < r_0 \\ \Big[1 + 9f(r), -\dfrac{f(r)u_0}{r_0}(x_2 - 0.5), \dfrac{f(r)u_0}{r_0}(x_1 - 0.5)\Big]^T, & r_0 \le r < r_1 \\ [1, 0, 0]^T, & r > r_1 \end{cases}$$

$$u_3 = 0, \ \mathbf{B} = \frac{5}{\sqrt{4\pi}}[1, 0, 0]^T, \ p = 1,$$

where $r = \sqrt{(x_1 - 0.5)^2 + (x_2 - 0.5)^2}$, $r_0 = 0.1$, $r_1 = 0.115$, $u_0 = 2$ *and* $f(r) = (r_1 - r)/(r_1 - r_0)$. *The ratio of the specific heats is* $\gamma = 1.4$. *The computational domain is* $\Omega = (0, 1) \times (0, 1)$ *and the final time is* $T = 0.15$.

This example, known as the first rotor problem, originates from Balsara and Spicer [1] and is presented in a modified form in [49]. Figure 7 displays the contours of the Mach number $|\boldsymbol{u}|/c$ (where $c = \sqrt{\gamma p/\rho}$ is the sound speed) and magnetic pressure. Notably, our scheme accurately captures the central rotating region without introducing any distortions. Furthermore, the numerical solution maintains the positivity of density and pressure without requiring any specialized positive-preserving limiter.

Example 7. *Consider the MHD Kelvin-Helmholtz instability problem in Yee and Sjögrenn [54] and reference therein. The computational domain is* $\Omega = (0, 1) \times (-1, 1)$ *with periodic boundary conditions. The initial condition data are*

$$\rho = 1.0,$$
$$u_1(x, y, 0) = 5\big(\tanh(20(y + 0.5)) - \tanh(20(y - 0.5)) - 1\big),$$

Figure 7: The profiles of Mach number and magnetic pressure of rotor problem in Example 6, $k = 2$, $T = 0.15$. 30 equally spaced contour lines are plotted: Mach number $|\boldsymbol{u}|/c \in [0.2, 4.0]$, magnetic pressure $|\boldsymbol{B}|^2/2 \in [0.2, 2.4]$.

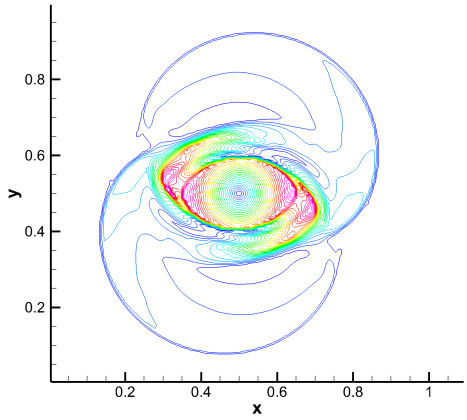

(a) $|\boldsymbol{u}|/c$, 128×128

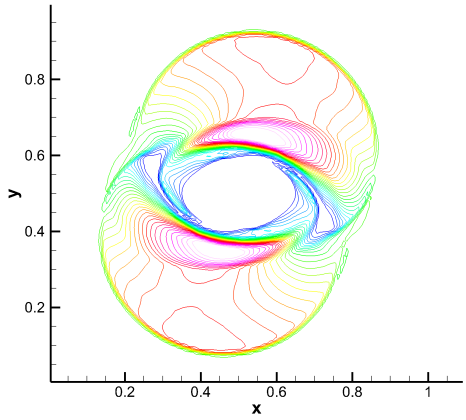

(b) $|\boldsymbol{B}|^2/2$, 128×128

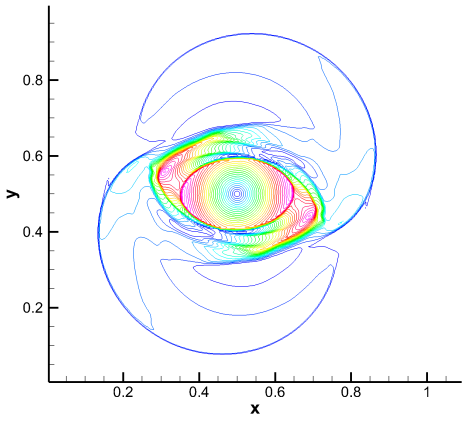

(c) $|\boldsymbol{u}|/c$, 256×256

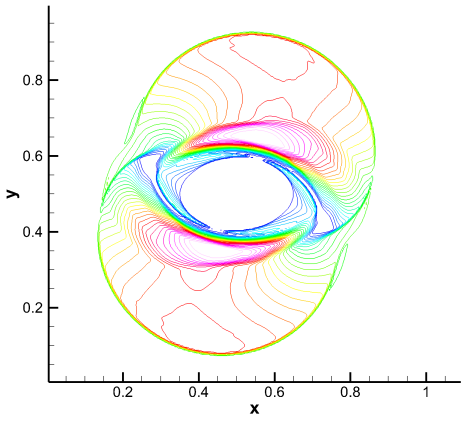

(d) $|\boldsymbol{B}|^2/2$, 256×256

$$u_2(x, y, 0) = 0.25 \sin(2\pi x)\big(e^{-100(y+0.5)^2} - e^{-100(y-0.5)^2}\big),$$
$$u_3 = 0, \ \mathbf{B} = [0, 0, 0]^T, \ p = 50.0\,.$$

The ratio of the specific heats is $\gamma = 1.4$ *and the final time is* $T = 0.5$.

Figure 8 displays contour plots of density, x-velocity, thermal pressure, and magnetic pressure for the problem under consideration. The simulation utilizes a computational mesh of 256×512 cells. The results clearly illustrate the growth of the magnetic field, which, being frozen into the fluid, is amplified by the vortical flow structures. The numerical scheme effectively resolves these complex features.

Figure 8: The profiles of density, x-velocity, thermal pressure, magnetic pressure of Kelvin Helmholtz instability problem in Example 7, $k = 2$, $T = 0.5$, $N_x \times N_y = 256 \times 512$. 30 equally spaced contour lines are plotted: density $\rho \in [0.67, 1.13]$, velocity $u_1 \in [-6, 6]$, thermal pressure $p \in [34, 59]$, magnetic pressure $|\boldsymbol{B}|^2/2 \in [1, 21]$.

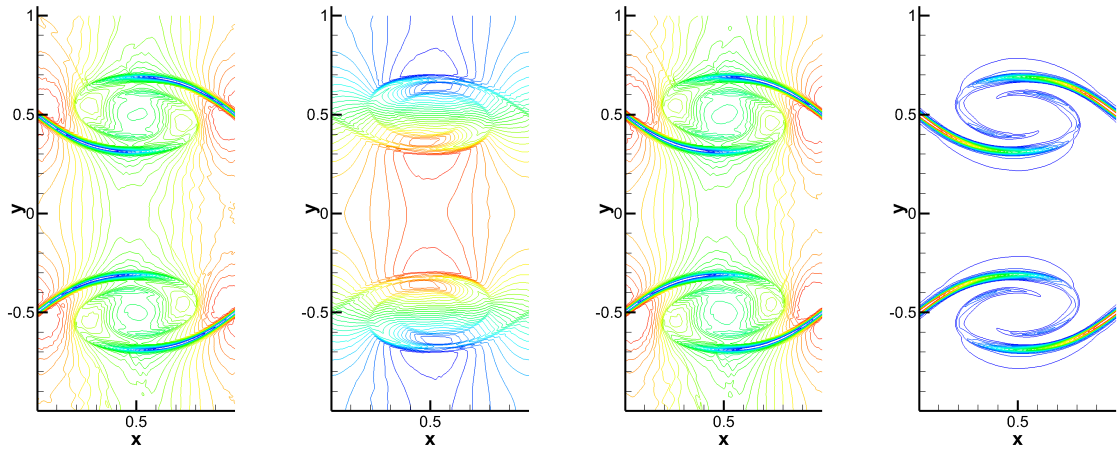

(a) ρ (b) u_1 (c) p (d) $|\boldsymbol{B}|^2/2$

Example 8. *Consider the blast problem in [1]. The initial condition is taken as*

$$\rho = 1,\ \mathbf{u} = [0,0,0]^T,\ \mathbf{B} = \frac{100}{\sqrt{4\pi}}[1,0,0]^T,\ p = \begin{cases} 1000, & r \le R \\ 0.1, & r > R \end{cases}$$

with $r = \sqrt{x_1^2 + x_2^2}$ *and* $R = 0.1$. *Outgoing boundary conditions are prescribed. The ratio of the specific heats is* $\gamma = 1.4$. *The computational domain is* $(-0.5, 0.5) \times (-0.5, 0.5)$ *and the final time is* $T = 0.01$.

Figure 9 showcases contours of density, thermal pressure, and magnetic pressure for the blast wave problem, illustrating its inherent complexity. As recognized in previous studies [1, 30, 31], this problem poses a significant challenge for numerical schemes. Our results demonstrate the efficacy of the proposed method, as it successfully captures the solution without resorting to artificial nonlinear limiters. Notably, the scheme maintains positivity of density and pressure even near the shock front.

Example 9. *Consider the cloud-shock interaction problem in [31] describing the strong MHD shocks interacting with a dense cloud. The computational domain is* $\Omega = (0, 2) \times (0, 1)$, *and it is divided into three regions initially:*

(1) *the post-shock region* $\Omega_1 = \{(x_1, x_2) : 0 \le x_1 \le 1.2,\ 0 \le x_2 \le 1\}$,

(2) *the pre-shock region* $\Omega_2 = \{(x_1, x_2) : 1.2 \le x_1 \le 2,\ 0 \le x_2 \le 1,\ r(x_1 - 1.4, x_2 - 0.5) \ge 0.18\}$,

Figure 9: The profiles of density, thermal pressure, and magnetic pressure of blast problem in Example 8, 256×256, $k = 2$, $T = 0.6$. 40 equally spaced contour lines are plotted: density $\rho \in [0.4, 4.6]$, thermal pressure $p \in [10, 250]$, magnetic pressure $|\boldsymbol{B}|^2/2 \in [215, 595]$.

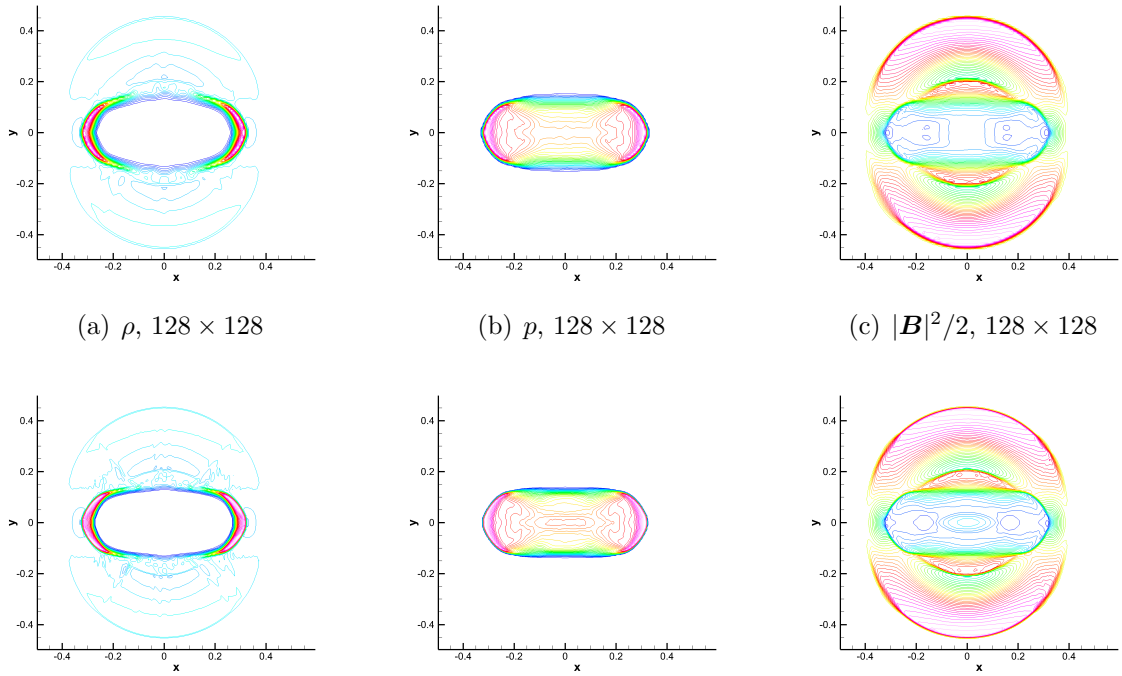

(a) ρ, 128×128 (b) p, 128×128 (c) $|\boldsymbol{B}|^2/2$, 128×128

(d) ρ, 256×256 (e) p, 256×256 (f) $|\boldsymbol{B}|^2/2$, 256×256

(3) *the cloud region* $\Omega_3 = \{(x_1, x_2) : r(x_1 - 1.4, x_2 - 0.5) < 0.18\}$.

where $r(x_1, x_2) = \sqrt{x_1^2 + x_2^2}$. *The initial condition in* Ω_1, Ω_2 *and* Ω_3 *are given as*

$$[\rho, u_1, u_2, u_3, B_1, B_2, B_3, p]^T = \begin{cases} [3.88968, 0, 0, -0.05234, 1, 0, 3.9353, 14.2641]^T, & \text{in } \Omega_1 \\ [1, -3.3156, 0, 0, 1, 0, 1, 0.04]^T, & \text{in } \Omega_2 \\ [5, -3.3156, 0, 0, 1, 0, 1, 0.04]^T, & \text{in } \Omega_3 \end{cases}$$

The ratio of the specific heats is $\gamma = 5/3$. *Outgoing boundary conditions are prescribed. The final time is* $T = 0.6$.

Figure 10 displays contour lines of density (ρ), thermal pressure (p), Mach number ($|\mathbf{u}|/c$), and magnetic pressure ($|\mathbf{B}|^2/2$) obtained by using the ESOFDG scheme on a 512×256 mesh at $T = 0.6$. The solution exhibits high resolution, accurately capturing discontinuities and complex flow structures without spurious oscillations. Our results align well with those presented in [31].

Example 10. *The final example explores two challenging MHD jet problems proposed in [53]. The static ambient gas is* $[\rho, p]^T = [0.1\gamma, 1]^T$ *with a magnetic field* $[0, B_2, 0]^T$ *inside*

Figure 10: The profiles of density, thermal pressure, Mach number, and magnetic pressure of cloud-shock interaction problem in Example 9, 512×256, $k = 2$, $T = 0.6$. 30 equally spaced contour lines are plotted: density $\rho \in [2.7, 11.1]$, thermal pressure $p \in [7.8, 14.1]$, Mach number $|\boldsymbol{u}|/c \in [0.04, 0.62]$, magnetic pressure $|\boldsymbol{B}|^2/2 \in [4.6, 11.4]$.

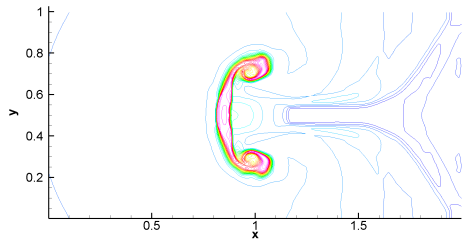

(a) ρ

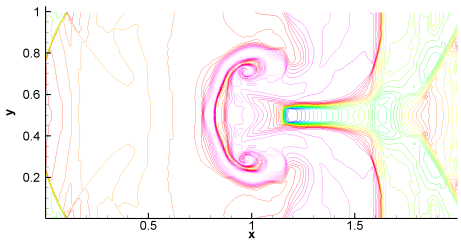

(b) p

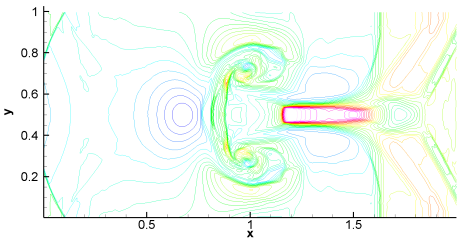

(c) $|\boldsymbol{u}|/c$

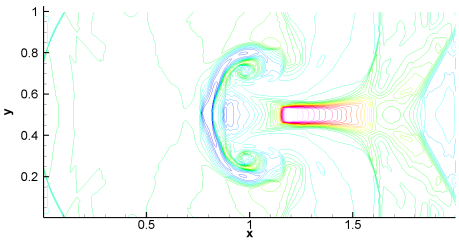

(d) $|\boldsymbol{B}|^2/2$

the domain $\Omega = (-0.5, 0.5) \times (0, 1.5)$. *The test becomes more and more challenging as* B_2 *increases, as observed in [53]. The boundary conditions are all outgoing except the inflow boundary condition at the nozzle* $\{|x| \leq 0.05, y = 0\}$. *We consider two kinds of initial settings as follows.*

I.C. (i) *First, we set* $B_2 = \sqrt{2000}$. *At the nozzle,* $[\rho, p]^T = [\gamma, 1]^T$, $\mathbf{u} = [0, 800, 0]^T$, *and the magnetic fields* $\mathbf{B} = [0, \sqrt{2000}, 0]^T$. *The adiabatic index is* $\gamma = 1.4$ *and the final time is* $T = 0.002$.

I.C. (ii) *Second, we set* $B_2 = \sqrt{20000}$. *At the nozzle,* $[\rho, p]^T = [\gamma, 1]^T$, $\mathbf{u} = [0, 10000, 0]^T$, *and the magnetic fields* $\mathbf{B} = [0, \sqrt{20000}, 0]^T$. *The adiabatic index is* $\gamma = 1.4$ *and the final time is* $T = 0.00015$.

In Example 10, the numerical simulation of MHD jet problems is quite challenging, due to the potential occurrence of negative density and pressure. To address this issue, we employ the positivity-preserving limiter [55] during the simulation. The CFL number is adjusted to $CFL = \frac{0.2}{(2k+1)}$ to prevent code breakdown. From Figures 11 and 12, we can see the proposed scheme effectively captures the Mach shock wave at the head of the jet. Notably, the flow structure near the beam/cocoon interfaces of jets is clearly presented with high resolution. The numerical results align well with those reported in

[53].

Figure 11: The profiles of density, y-velocity, and magnetic pressure of Mach 800 MHD jet problem in Example 10, $k = 2$, $T = 0.002$, $N_x \times N_y = 320 \times 480$. 40 equally spaced contour lines are plotted: density logarithm $\rho \in [-1.58, 1.12]$, velocity $u_2 \in [-40, 790]$, magnetic pressure logarithm $\log_{10}\left(|\mathbf{B}|^2/2\right) \in [-1.6, 3.6]$.

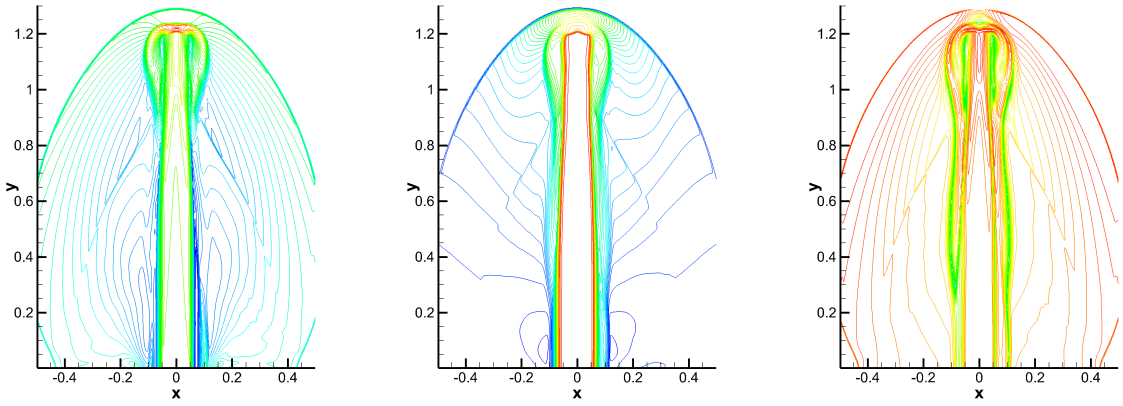

(a) $\log_{10}\rho$ (b) u_2 (c) $\log_{10}\left(|\mathbf{B}|^2/2\right)$

Figure 12: The profiles of density, y-velocity, and magnetic pressure of Mach 10000 MHD jet problem in Example 10, $k = 2$, $T = 0.00015$, $N_x \times N_y = 320 \times 480$. 40 equally spaced contour lines are plotted: density logarithm $\log_{10}\rho \in [-1.8, 0.9]$, velocity $u_2 \in [-500, 10000]$, magnetic pressure logarithm $\log_{10}\left(|\mathbf{B}|^2/2\right) \in [-0.8, 5.2]$.

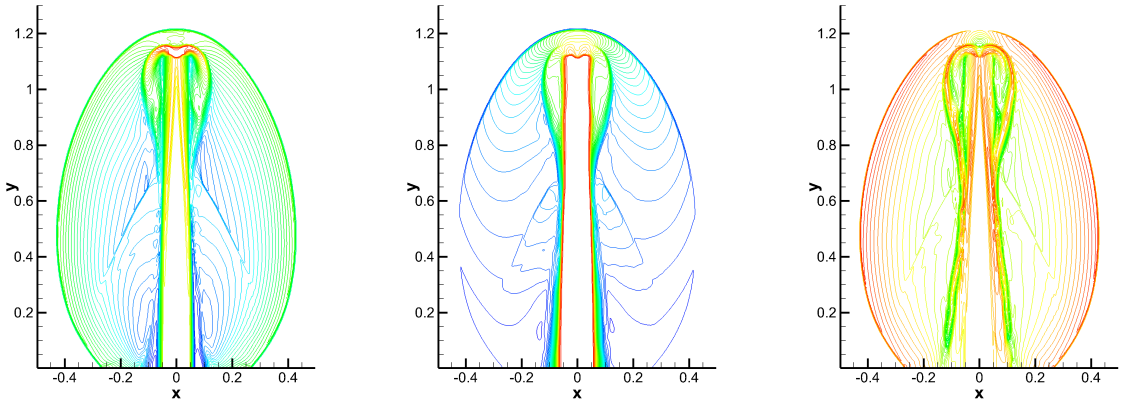

(a) $\log_{10}\rho$ (b) u_2 (c) $\log_{10}\left(|\mathbf{B}|^2/2\right)$

5 Concluding remarks

This paper extends our previously developed entropy-stable oscillation-free discontinuous Galerkin (ESOFDG) method to solve the ideal magnetohydrodynamics (MHD) equations. To ensure entropy stability for the MHD system, we employ a non-conservative formulation of the MHD system with the incorporation of Godunov's source term. Based on the ESOFDG method, we introduce a novel damping term specifically designed for the MHD equations to achieve entropy stability in the semi-discrete case. This damping term can achieve both the entropy stability and the oscillation-free property simultaneously. We utilize a time-splitting and semi-implicit approach to implement the additional damping term, ensuring that the original CFL condition is maintained even for problems involving strong shocks. Numerical examples are presented to verify the robustness and efficiency of the proposed method.

References

[1] D.S. Balsara and D.S. Spicer. *A staggered mesh algorithm using high order Godunov fluxes to ensure solenoidal magnetic fields in magnetohydrodynamic simulations*. J. Comput. Phys. 149 (1999), pp. 270 – 292.

[2] D.S. Balsara and R. Käppeli. *Von Neumann stability analysis of globally divergence-free RKDG schemes for the induction equation using multidimensional Riemann solvers*. J. Comput. Phys. 336 (2017), pp. 104 – 127.

[3] M.W. Bohm, A.R. Winters, G.J. Gassner, D. Derigs, F.J. Hindenlang, and J. Saur. *An entropy stable nodal discontinuous Galerkin method for the resistive MHD equations. Part I: Theory and numerical verification*. J. Comput. Phys. 422 (2020), 108076.

[4] F. Brackbill and D. Barnes. *The effect of nonzero* $\nabla \cdot \mathbf{B}$ *on the numerical solution of the magnetohydrodynamic equations*. J. Comput. Phys. 35 (1988), pp. 426 – 430.

[5] M. Brio, C.C. Wu, *An upwind differencing scheme for the equations of ideal magnetohydrodynamics*. J. Comput. Phys. 75 (1988) pp. 400 – 422.

[6] J. Crean, J.E. Hicken, D.C. Del Rey Fernández, D.W. Zingg, and M.H. Carpenter, *High order, entropy-stable discretizations of the Euler equations for complex geometries*. in Proceedings of the 23rd AIAA Computational Fluid Dynamics Conference, 2017.

[7] J. Crean, J.E. Hicken, D.C. Del Rey Fernández, D.W. Zingg, and M.H. Carpenter. *Entropy stable summation-by-parts discretization of the Euler equations on general curved elements*. J. Comput. Phys. 356 (2018), pp. 410 – 438.

[8] J. Chan. *On discretely entropy conservative and entropy stable discontinuous Galerkin methods*. J. Comput. Phys. 362 (2018), pp. 346 – 374.

[9] J. Chan, D.C. Del Rey Fernández, and M.H. Carpenter. *Efficient entropy stable Gauss collocation methods*. SIAM J. Sci. Comput. 41 (2019), pp. A2938–A2966.

[10] P. Chandrashekar and C. Klingenberg. *Entropy stable finite volume scheme for ideal compressible MHD on 2-D Cartesian meshes*. SIAM J. Numer. Anal. 54 (2016), pp. 1313 – 1340.

[11] T. Chen and C.-W. Shu. *Entropy stable high order discontinuous Galerkin methods with suitable quadrature rules for hyperbolic conservation laws*. J. Comput. Phys. 345 (2017), pp. 427 – 461.

[12] T. Chen and C.-W. Shu. *Review of entropy stable discontinuous Galerkin methods for systems of conservation laws on unstructured simplex meshes*. CSIAM Trans. Appl. Math. 1 (2020), pp. 1 – 52.

[13] Y. Cheng and C.-W. Shu. *A discontinuous Galerkin finiite element method for directly solving the Hamilton–Jacobi equations*. J. Comput. Phys. 223 (2007), pp. 398 – 415.

[14] B. Cockburn and C.-W. Shu. *TVB Runge-Kutta local projection discontinuous Galerkin finite element method for scalar conservation laws II: General framework*. Math. Comp. 52 (1989), pp. 411 – 435.

[15] A. Dedner, F. Kemm, D. Kröner, C.D. Munz, T. Schnitzer, and M. Wesenberg. *Hyperbolic divergence cleaning for the MHD equations*. J. Comput. Phys. 175 (2002), pp. 645 – 673.

[16] D. Derigs, A.R. Winters, G.J. Gassner, and S. Walch. *A novel averaging technique for discrete entropy stable dissipation operators for ideal MHD*. J. Comput. Phys. 330 (2016), pp. 624 – 632.

[17] D. Derigs, A.R. Winters, G.J. Gassner, S. Walch, and M. Bohm. *Ideal GLM-MHD: About the entropy consistent nine-wave magnetic field divergence diminishing ideal magnetohydrodynamics equations*. J. Comput. Phys. 364 (2018), pp. 420 – 467.

[18] D.C. Del Rey Fernández, J. E. Hicken, and D. W. Zingg. *Simultaneous approximation terms for multi-dimensional summation-by-parts operators*. J. Sci. Comput. 75 (2018), pp. 83 – 110.

[19] J. Du, Y. Liu, and Y. Yang. *An oscillation-free bound-preserving discontinuous Galerkin method for multi-component chemically reacting flows*. J. Sci. Comput. 95 (2023), Paper No. 90.

[20] C.R. Evans and J.F. Hawley. *Simulation of magnetohydrodynamic flows – a constrained transport method*. Astrophys. J. 332 (1988), pp. 659 – 677.

[21] M. Fey and M. Torrilhon. *A constrained transport upwind scheme for divergence-free advection*. in: Hyperbolic Problems: Theory, Numerics, Applications. Springer, Berlin, Heidelberg, 2003, pp. 529 – 538.

[22] U.S. Fjordholm, S. Mishra, and E. Tadmor. *Arbitrarily high-order accurate entropy stable essentially nonoscillatory schemes for systems of conservation laws*. SIAM J. Numer. Anal. 50 (2012), pp. 544 – 573.

[23] U. S. Fjordholm, S. Mishra, and E. Tadmor. *ENO reconstruction and ENO interpolation are stable*. Found. Comput. Math. 13 (2013), pp. 139 – 159.

[24] E. Godlewski and P. Raviart. *Numerical Approximation of Hyperbolic Systems of Conservation Laws*. Springer, 1996.

[25] S.K. Godunov. *The symmetric form of magnetohydrodynamics equations*. in: Numerical Methods for Mechanics of Continuum Medium, 1 (1972), pp. 26 – 34.

[26] C. Helzel, J.A. Rossmanith, and B. Taetz. *An unstaggered constrained transport method for the 3D ideal magnetohydrodynamic equations*. J. Comput. Phys. 230 (2011), pp. 3803 – 3829.

[27] J.E. Hicken, D.C. Del Rey Fernández, and D.W. Zingg. *Multidimensional summation-by-parts operators: General theory and application to simplex elements*. SIAM J. Sci. Comput. 38 (2016), pp. A1935 – A1958.

[28] R. Hiptmair, L. Li, S. Mao, and W. Zheng. *A fully divergence-free finite element method for magnetohydrodynamic equations*. Math. Models Methods Appl. Sci. 28 (2018), pp. 659 – 695.

[29] P. G. Lefloch, J.-M. Mercier, and C. Rohde. *Fully discrete, entropy conservative schemes of arbitrary order*. SIAM J. Numer. Anal. 40 (2002), pp. 1968 – 1992.

[30] S. Li. *High order central scheme on overlapping cells for magneto-hydrodynamic flows with and without constrained transport method.* J. Comput. Phys. 227 (2008), pp. 7368 – 7393.

[31] F. Li and L. Xu. *Arbitrary order exactly divergence-free central discontinuous Galerkin methods for ideal MHD equations.* J. Comput. Phys. 231 (2012), pp. 2655 – 2675.

[32] Y. Liu, J. Lu, Q. Tao, and Y. Xia. *An oscillation-free discontinuous Galerkin method for shallow water equations.* J. Sci. Comput. 92 (2022), Paper No. 109.

[33] Y. Liu, J. Lu, and C.-W. Shu. *An essentially oscillation-free discontinuous Galerkin method for hyperbolic systems.* SIAM J. Sci. Comput. 44 (2022), pp. A230 – A259.

[34] Y. Liu, J. Lu, and C.-W. Shu. *An entropy stable essentially oscillation-free discontinuous Galerkin method for hyperbolic conservation laws.* SIAM J. Sci. Comput. 46(2024), pp. A1132 – A1159.

[35] Y. Liu, C.-W. Shu, and M. Zhang. *Entropy stable high order discontinuous Galerkin methods for ideal compressible MHD on structured meshes.* J. Comput. Phys. 354 (2018), pp. 163 –178.

[36] J. Lu, Y. Liu, and C.-W. Shu. *An oscillation-free discontinuous Galerkin method for scalar hyperbolic conservation laws.* SIAM J. Numer. Anal. 59 (2021), pp. 1299 – 1324.

[37] C. D. Munz, P. Omnes, R. Schneider, E. Sonnendrücker, and U. Voß. *Divergence Correction Techniques for Maxwell Solvers Based on a Hyperbolic Model.* J. Comput. Phys. 161 (2000), pp. 484 – 511.

[38] J.-X. Qiu and C.-W. Shu. *Runge–Kutta discontinuous Galerkin method using WENO limiters.* SIAM J. Sci. Comput. 26 (2005), pp. 907 – 929.

[39] K.G. Powell. *An approximate Riemann solver for magnetohydrodynamics, in: Upwind and High-Resolution Schemes.* Springer, Berlin, Heidelberg, 1997, pp. 570 – 583.

[40] M. Peng, Z. Sun, and K. Wu. *OEDG: Oscillation-eliminating discontinuous Galerkin method for hyperbolic conservation laws.* Math. Comp. (2024). https://doi.org/10.1090/mcom/3998

[41] J.A. Rossmanith. *An unstaggered, high-resolution constrained transport method for magnetohydrodynamic flows.* SIAM J. Sci. Comput. 28 (2006), pp. 1766 – 1797.

[42] D. Ryu and T.W. Jones *Numerical Magnetohydrodynamics in Astrophysics: Algorithm and Tests for Multi-Dimensional Flow 1.* Astrophys. J. 442 (1995), pp. 228 – 258.

[43] C.-W. Shu. *TVB uniformly high-order schemes for conservation laws.* Math. Comp. 49 (1987), pp. 105 – 121.

[44] C.-W. Shu and S. Osher. *Efficient implementation of essentially non-oscillatory shock-capturing schemes.* J. Comput. Phys. 77 (1988), pp. 439 – 471.

[45] C.-W. Shu. *Total-Variation-Diminishing time discretizations.* SIAM J. Sci. Stat. Comput. 9 (1988), pp. 1073 – 1084.

[46] E. Tadmor. *The numerical viscosity of entropy stable schemes for systems of conservation laws.* Math. Comp. 49 (179) (1987), pp. 91 – 103.

[47] E. Tadmor. *Entropy stability theory for difference approximations of nonlinear conservation laws and related time-dependent problems.* Acta Numer. 12 (2003), pp. 451 – 512.

[48] Q. Tao, Y. Liu, Y. Jiang, and J. Lu. *An oscillation-free local discontinuous Galerkin method for nonlinear degenerate parabolic equations.* Numer. Methods Partial Differ. Equ. 39 (2023), pp. 3145 – 3169.

[49] G. Tóth. *The $\nabla \cdot \mathbf{B} = 0$ constraint in shock-capturing magnetohydrodynamics codes.* J. Comput. Phys. 161 (2000), pp. 605 – 652.

[50] A. R. Winters, D. Derigs, G. J. Gassner, and S. Walch. *A uniquely defined entropy stable matrix dissipation operator for high Mach number ideal MHD and compressible Euler simulations.* J. Comput. Phys. 332 (2017), pp. 274 – 289.

[51] A.R. Winters and G.J. Gassner. *Affordable, entropy conserving and entropy stable flux functions for the ideal MHD equations.* J. Comput. Phys. 304 (2016), pp. 72 – 108.

[52] K. Wu. *Positivity-preserving analysis of numerical schemes for ideal magnetohydrodynamics.* SIAM J. Numer. Anal. 56 (2018), pp. 2124 – 2147.

[53] K. Wu and C.-W. Shu. *A provably positive discontinuous Galerkin method for multidimensional ideal magnetohydrodynamics.* SIAM J. Sci. Comput. 40 (2018), pp. B1302 – B1329.

[54] H.C. Yee and B. Sjögreen. *Divergence free high order filter methods for the compressible MHD equations*, in: Proceedings of the International Conference on High

Performance Computing, March 10-14, 2003, Hanoi, Vietnam. Springer, Berlin, Heidelberg, 2005, pp. 559 – 575.

[55] X. Zhang and C.-W. Shu. *On maximum-principle-satisfying high order schemes for scalar conservation laws*. J. Comput. phys. 229 (2010), pp. 3091 – 3120.

[56] X. Zhong and C.-W. Shu. *A simple weighted essentially nonoscillatory limiter for Runge-Kutta discontinuous Galerkin methods*, J. Comput. phys. 232 (2013), pp. 397 – 415.

[57] H. Zuo, W. Zhao, and P. Lin. *A positivity preserving and oscillation-free entropy stable discontinuous Galerkin scheme for the reactive Euler equations*. J. Comput. phys. 505 (2024), 112906.